12. Meyerson B. Comments on North RB, Calkins S-K, Campbell DS et al. Automated, patient-interactive, spinal cord stimulator adjustment: a randomized controlled trial. *Neurosurgery* 2003;52:580.

13. Budd K. Spinal cord stimulation: cost-benefit study. *Neuromodulation* 2002;5:75–78.

14. North RB, Kidd D, Shipley J, Taylor RS. Spinal cord stimulation versus reoperation for failed back surgery syndrome: a cost effectiveness and cost utility analysis based on a randomized, controlled trial. *Neurosurgery* 2007;61:361–368; discussion 368–369.

15. Kumar K, Malik S, Demeria D. Treatment of chronic pain with spinal cod stimulation versus alternative therapies: cost-effectiveness analysis. *Neurosurgery* 2002;51:106–111; discussion 115–116.

16. Andrell P, Ekre O, Eliasson T et al. Cost-effectiveness of spinal cord stimulation versus coronary artery bypass grafting pin patients with severe angina pectoris—long-term results from the ESBY study. *Cardiology* 2003;99:20–24.

17. Kemler MA, Furnee CA. Economic evaluation of spinal cord stimulation for chronic reflex sympathetic dystrophy. *Neurology* 2002;59:1203–1209.

Volume 11 • Number 3 • 2008
http://www.blackwell-synergy.com/loi/ner

ORIGINAL ARTICLE

c-Fos Expression After Chronic Electrical Stimulation of Sensorimotor Cortex in Rats

Katsunori Shijo, MD • Yoichi Katayama, MD, PhD • Akiko Yamashita, PhD • Kazutaka Kobayashi, MD, PhD • Hideki Oshima, MD, PhD • Chikashi Fukaya, MD, PhD • Takamitsu Yamamoto, MD, PhD

Department of Neurological Surgery, Nihon University School of Medicine and Division of Applied System Neuroscience, Graduate School of Medical Science, Tokyo, Japan

ABSTRACT

Objectives. Motor cortex stimulation has been used as a treatment for intractable pain. However, the mechanisms underlying its effects remain unclear. In this study, neuroplasticity induced by chronic sensorimotor cortex stimulation was investigated experimentally on the basis of *c-Fos* expression. **Materials and Methods.** The experimental animals employed were adult male Wistar rats. A quadripolar stimulation electrode was positioned over the sensorimotor cortex. We examined the neural activation in response to chronic stimulation using *c-Fos* immunopositivity. **Results.** The results are as follows: 1) *c-Fos* was significantly expressed immediately after the stimulation compared with that in the control; 2) *c-Fos* expression became extensive over the various regions with an increase in stimulation duration; and 3) after two months of stimulation, *c-Fos* was expressed not only on the stimulation side, but also within the contralateral cerebral hemisphere. **Conclusions.** Changes in *c-Fos* expression induced by long-term stimulation indicate the existence of a time-dependent neural plasticity.

KEY WORDS: c-Fos, *motor cortex stimulation, neural plasticity, rat, sensorimotor cortex.*

Introduction

Motor cortex stimulation (MCS) was introduced by Tsubokawa et al. (1) and Katayama et al. (2) as a treatment for intractable thalamic pain. Following their reports, such treatment has been applied to the treatment of peripheral neuropathic pain, and involuntary movements, and very recently to poststroke hemiparesis. Long-term observations have indicated that beneficial effects of chronic MCS can be achieved in many patients with neurologic dysfunction. However, the mechanisms underlying these therapeutic effects have not yet been clarified.

The distribution of neural activity in relation to the motor function is highly dynamic and changes in response to various manipulations, including differential motor training (3–5), the administration of various pharmacologic agents and electrical cortical stimulation (6,7). It is intriguing to speculate that electrical cortex stimulation can cause a functional reorganization and a change in the neurocircuitry. In particular, repeated intracortical microstimulations (6) and kindling (7) have been shown to induce significant motor map expansion in animal experiments.

On the other hand, there are a number of recent studies indicating that gene expression in neurons and glial cells is markedly up-regulated following periods of intense neural activity (8,9). Such stimulation induces a rapid and transient expression of immediate-early genes (IEG) in

Submitted: August 14, 2006; accepted: April 15, 2008. Address correspondence and reprint requests to: Chikashi Fukaya, MD, PhD, Department of Neurological Surgery, Nihon University School of Medicine, Oyaguchi-Kamimachi 30-1, Itabashi-ku, Tokyo 173-8610, JAPAN. Email: chikashi@med.nihon-u.ac.jp

the brain, and the monitoring of IEGs has enabled the visualization of neural plasticity induced by electric stimulation. Many IEGs are transcription factors that directly control the expression of other secondary response genes (10). We investigated the activation of the cortex and related nuclei in response to the chronic electrical stimulation of the sensorimotor cortex using *c-Fos* immunopositivity as a marker of neural activity.

Materials and Methods

This study was carried out in accordance with the Guidelines for Animal Experimentation of the Faculty of Medicine, Nihon University.

Surgical Procedure and Electrical Stimulation

The experimental animals used were 20 adult male Wistar rats (body weight, 300–600 g). The animals were anesthetized for consistency using ketamine hydroxylase (100 mg/kg body weight, intramuscularly) and a mixture of 0.5% epinephrine hydrochloride and lidocaine hydrochloride (1 mL each), injected subcutaneously and below the external ear canals to numb the areas. Then, pentobarbital (Nembutal, Abbott Laboratories, Chicago, IL, USA; 20 mg/kg body weight, intraperitoneally) was injected. After the electrical stimulation parameters were fixed, Nembutal was re-injected.

Each rat was positioned in a stereotactic frame and a cranial burr hole (2 mm × 5 mm) was drilled on the left coronal suture 3.5 mm lateral to the midline (Fig. 1).

A novel quadripolar stimulation electrode (2 mm wide, 5 mm long) was positioned over the sensorimotor cortex. The electrode with four contact points, numbered 0–3 sequentially from the most distal contact 0 to the most proximal contact 3, was placed in such a way that contact 0 was located in the rostral portion of the sensorimotor cortex. Each contact of the electrode was 0.7 mm long; the contacts were 0.7 mm apart.

Anodal pulses were applied at a 25-Hz frequency. The cathode was placed on the caudal side. A stimulation voltage in the range of 2–5 V was applied with an impulse duration of 0.12 msec. The voltage was determined to be less than 80% that required for forelimb muscle contraction. Extension wires were passed from the head to the back subcutaneously and connected to an implantable pulse generator (Soletora Model 7426 IPG, Medtronic Inc., Minneapolis, MN, USA). Stimulation was applied for three hours, two weeks, one month, and two months. Each group consisted of three animals. As control experiments, we carried out the same operative procedures on rats without electrical stimulation and reared the animals for periods matching those for the stimulated rats.

Evaluation of *c-Fos*-Positive Cells

Immunohistochemical analysis was carried out to visualize the localization of *c-Fos*-positive cells within the cerebrum.

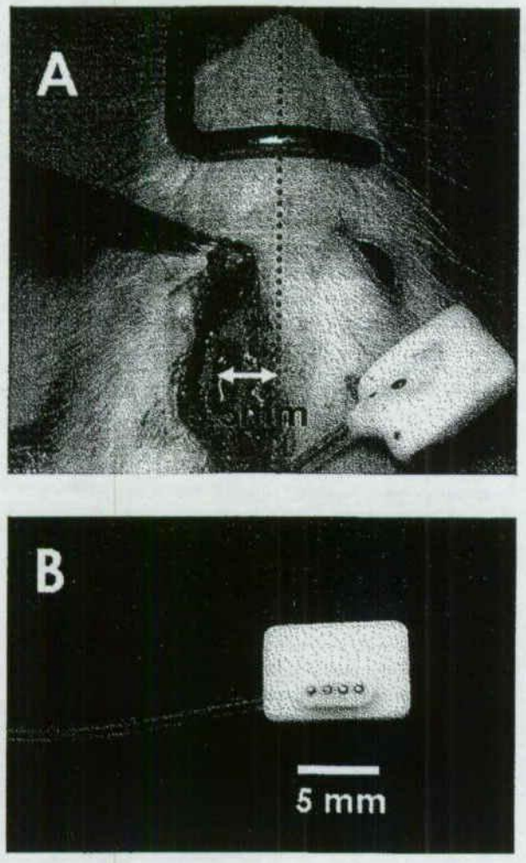

FIGURE 1. Each rat was positioned in a stereotactic frame and a cranial burr hole (2 mm × 5 mm: arrow) was drilled on the left coronal suture 3.5 mm lateral to the midline (A). A novel quadripolar stimulation electrode (2 mm wide, 5 mm long) was positioned over the sensorimotor cortex. Each contact of the electrode was 0.7 mm long; the contacts were 0.7 mm apart (B).

After the stimulation, the rats were killed by administering intraperitoneal pentobarbital (60 mg/kg body weight) and perfusing them with 4% paraformaldehyde in 0.1 M phosphate-buffered saline (pH 7.4). The extracted brains were postfixed in the same fixative for 12 hours with constant shaking, and then successively immersed in 10% and 20% sucrose for approximately 48 hours each at 4° until the brains were settled at the bottom of the solution. The brains were embedded in an optimal cutting temperature compound, frozen, and sectioned (40 μm thick) on a sliding microtome.

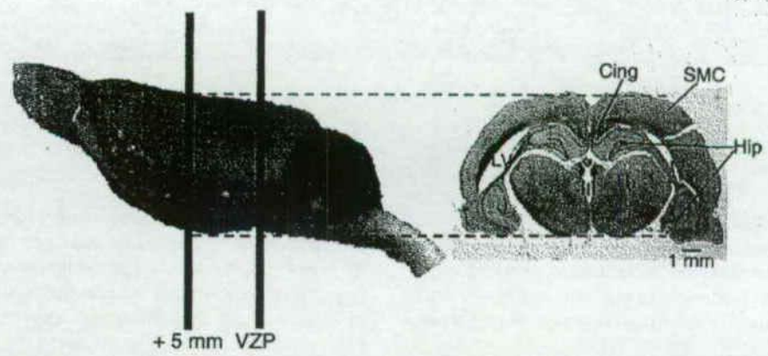

FIGURE 2. A parallel slice was made about 5 mm anterior to the VZP (vertical zero plane), which just included the stimulated part of the sensorimotor cortex. SMC, sensorimotor cortex; Th, thalamus; Cing, cingulate gyrus; Hip, hippocampus; III, third ventricle; LV, lateral ventricle; cc, corpus callosum. Bar = 1 mm.

Free-floating sections for *c-Fos* immunohistochemical analysis were pretreated with 0.3% H_2O_2 in methanol for 30 min and incubated in 1% normal goat serum and 10% fish gelatin in phosphate buffer (FG-PB, pH 7.4) for 30 min. They were then reacted with sheep anti-*c-Fos* antiserum (diluted 1 : 2000 in FG-PB, Chemicon, Temecula, CA, USA) for 48 hours in a refrigerator with constant shaking. After several washes with PB, the sections were reacted with a goat anti-sheep immunoglobulin G (IgG) secondary antibody (Vectastain ABC Elite kit, Vector Laboratories, Burlingame, CA, USA) for two hours at room temperature. Next, the sections were incubated with ABC solution (ABC kit) and reacted with 0.02% 3,3'-diaminobenzidine and 0.03% H_2O_2 for 10 min. Some selected sections were stained with neutral red for counterstaining. Neighboring sections were stained by conventional Nissl staining employing crystal violet. The sections were mounted on gelatin-coated glass slides, air-dried, dehydrated in ethanol, cleared in xylene and coverslipped (Fig. 2).

The sections were observed and photographed using a Coolscope CCD camera (Nikon, Tokyo, Japan) attached to an Eclipse microscope (Nikon). High magnification photographs were constructed employing picture processing software ACT1 (Nikon). The distribution of *c-Fos*-positive cells was plotted using a Neurolucida system (MicroBrightField, Williston, VT, USA) installed on a personal computer attached to an AX-10 microscope (Olympus, Tokyo, Japan) and a 2400c CCD camera (Hamamatsu Photonics, Hamamatsu, Japan).

Types of *c-Fos*-Immunoreactive Cell

To confirm cell type, we also used fluorescence double-staining. Ionized calcium-binding adaptor molecule 1 (Iba1) was used as a marker of microglia/macrophages (11), the glial fibrillary acidic protein (GFAP) was used as a marker of astrocytes, and neuron-specific enolase (NSE) and microtubule-associated protein 2 (MAP2) were used as markers of neurons. Selected sections were pretreated with 0.3% hydrogen peroxide in methanol and incubated in normal goat/horse/donkey serum and FG-PB (pH, 7.4). Then, the sections were incubated for 48 hours at 4° with anti-Iba1 rabbit antiserum (Wako, Osaka, Japan; final dilution of 1 : 200) or an anti-GFAP (Chemicon; 1 : 100) mouse antibody or an anti-NSE mouse antibody (Laboratory Vision Corporation, Fremont, CA, USA; 1 : 1000) diluted in FG-PB.

To visualize the immunoreactive sites, the sections were reacted with diaminobenzidine (DAB) and hydrogen peroxide solution. After treatment with an ABC blocking kit (Vector), the sections were reacted with an anti-*c-Fos* sheep antibody, as mentioned above, and hydrogen peroxide solution with cobalt chloride was used for visualization. For immunofluoresence study, some of the sections were incubated for 48 hours at 4° with a mixture of anti-*c-Fos* sheep antiserum and an anti-MAP2 mouse antibody (Sigma, St. Louis, MO, USA; 1 : 2000) diluted in FG-PB. The sections were reacted with a cocktail of secondary antibodies: a rhodamine-labeled anti-mouse IgG horse antibody (Vector) and an fluorescein isothiocyanate-labeled anti-sheep IgG donkey antibody (Chemicon). The sections were set on a glass slide and mounted in nonfluorescent glycerine (Merck, Darmstadt, Germany).

Detection of Degenerating Neurons

To detect degenerating neurons, Fluoro-Jade B (FJB) staining was carried out in accordance with the method of Schmued et al. (12). The sections were treated with 1% sodium hydroxide in 80% ethanol for 5 min and in 0.06% potassium permanganate for 10 min on a shaker. They

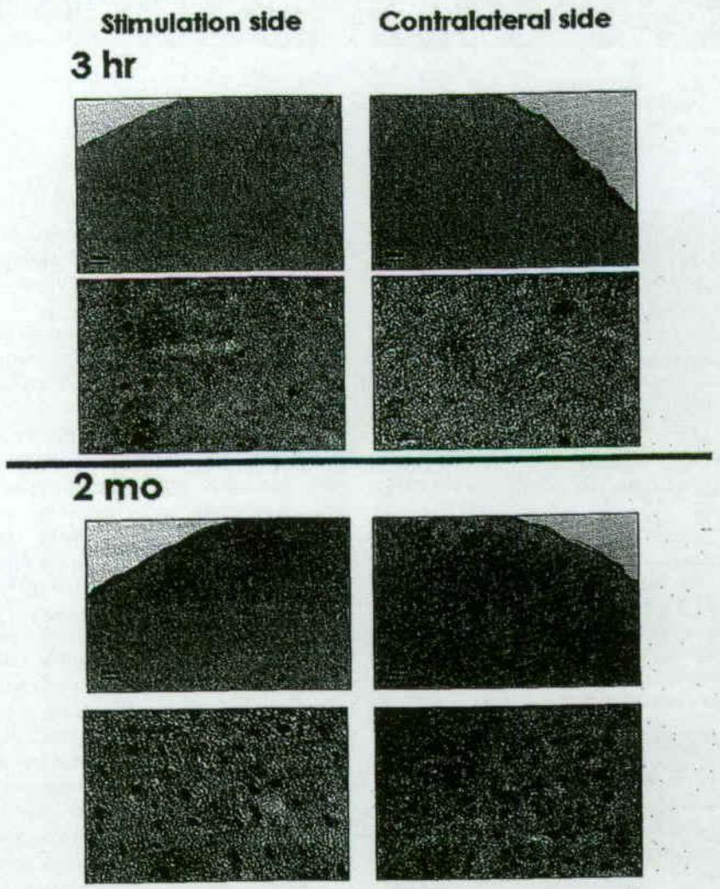

FIGURE 3. *c-Fos*-immunopositive cells observed microscopically in sensorimotor cortex on sides ipsilateral and contralateral to stimulation for three hours and two months of stimulation. Bars = above, 100 μm; below, 20 μm.

were then incubated in freshly mixed 0.0004% FJB (Cosmobio, Tokyo, Japan) in 0.1% acetic acid for 20 min, washed in distilled water and air-dried at 50° for 10 min. The sections were cleaned using xylene and coverslipped.

Results

In the sensorimotor cortex, few FJB-positive cells were observed for all experimental periods, indicating that no cell death was induced by the electrical stimulation in this study (data not shown). Moreover, only small numbers of *c-Fos*-positive cells were detected in the surgically operated control animals without stimulation, showing that *c-Fos* is mostly activated by the electrical stimulation. Compared with that in the control animals, a high density of *c-Fos*-immunopositive cells was observed in the rats subjected to three hours to two months of electrical stimulation of the sensorimotor cortex. Because the immunopositivity for *c-Fos* was found to be perinuclear in the cells, it was difficult to determine whether the immunopositive cells were neurons or glia. In the white matter and corpus callosum, observed *c-Fos*-immunopositive cells less than 10 μm in diameter indicated that at least some of the *c-Fos*-immunopositive cells were glia. On the other hand, in the gray matter, *c-Fos*-immunopositive cells with large somata also were (more than 20 μm in diameter) observed (Fig. 3). In the cortical gray matter, NSE/MAP2 and *c-Fos* double-stained cells were observed (Fig. 4A and B, respectively), indicating that this IEG is expressed in the neuronal cells in the cortex. On

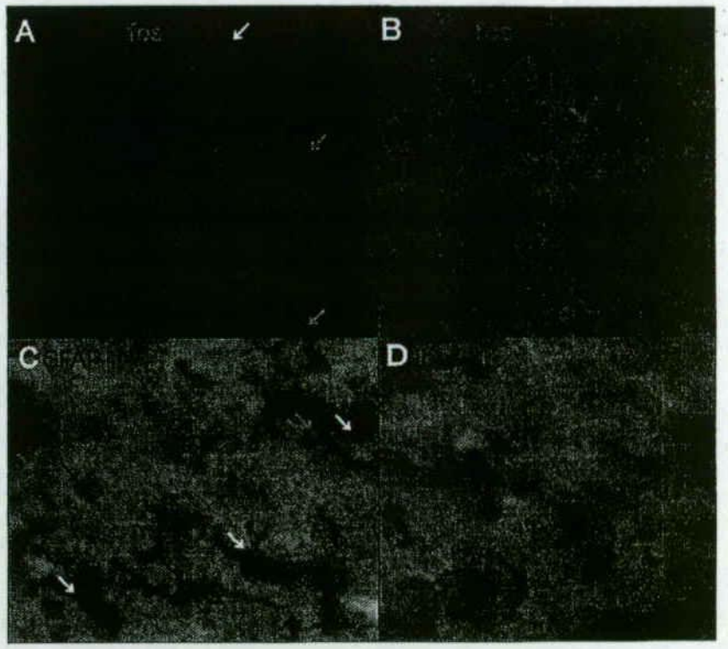

FIGURE 4. In layers II/III of the motor cortex after two months stimulation, MAP2-positive cells showed *c-Fos* immunoreactivity (yellow arrow). There were also MAP2-positive/*c-Fos*-negative neurons (red arrow) were also observed. MAP2 (green arrows in A) or neuron-specific enolase (NSE)-negative (blue arrow in B)/*c-Fos*-positive cells also were observed, suggesting that astrocytes also express *c-Fos*. At the border between the gray matter of the motor cortex and the white matter, glial fibrillary acidic protein (GFAP)-positive/*c-Fos*-positive (yellow arrows in C), GFAP-positive/*c-Fos*-negative (black arrows) and GFAP-negative/*c-Fos*-positive (blue arrows) cells were observed, indicating that both neurons and astrocytes express *c-Fos*. We detected no Iba1-positive cells showing *c-Fos* immunoreactivity (D). Bars = 20 μm.

TABLE 1. Numbers of *c-Fos*-Immunopositive Cells After Stimulation

		Nonstimulation $N=3$	3 Hours $N=3$	2 Weeks $N=3$	1 Month $N=3$	2 Months $N=3$
SMC	I	37.00 ± 22.91	148.67 ± 139.01	170.33 ± 59.68*	111.75 ± 41.55*	165.67 ± 88.23*
	C	35.67 ± 19.60	56.33 ± 40.50	92.33 ± 38.32*	92.00 ± 38.32*	193.00 ± 107.59*
Th	I	14.67 ± 12.74	112.67 ± 77.02*	113.67 ± 60.62*	91.00 ± 66.15*	134.00 ± 91.33*
	C	25.67 ± 9.81	75.67 ± 52.69	49.00 ± 22.61	118.50 ± 52.82*	197.33 ± 92.12*
Cing	I	41.67 ± 40.50	85.33 ± 15.01	150.67 ± 109.35	84.50 ± 64.26	108.33 ± 86.33
	C	21.33 ± 17.04	53.67 ± 25.58	103.33 ± 108.65	91.75 ± 51.10*	186.67 ± 84.03*

Asterisks, significantly different from nonstimulation; *$p < 0.05$, Mann–Whitney *U*-test.
SMC, sensorimotor cortex; Th, thalamus; Cing, cingulate gyrus; I, side ipsilateral to stimulation; C, side contralateral to stimulation.

the other hand, both GFAP-negative (blue arrows in Fig. 4C) and GFAP-positive cells (yellow arrows, Fig. 4C) expressing *c-Fos* immunoreactivity were observed, indicating that both neurons and astrocytes show the transcription of a new gene. No Iba1 and *c-Fos* double-stained cells were detected (Fig. 4D). We concluded, therefore, that both neurons and glia are *c-Fos*-immunopositive.

The distribution pattern of *c-Fos*-immunopositive cells is summarized in Table 1. It changed significantly depending on stimulation duration (Mann–Whitney *U*-test).

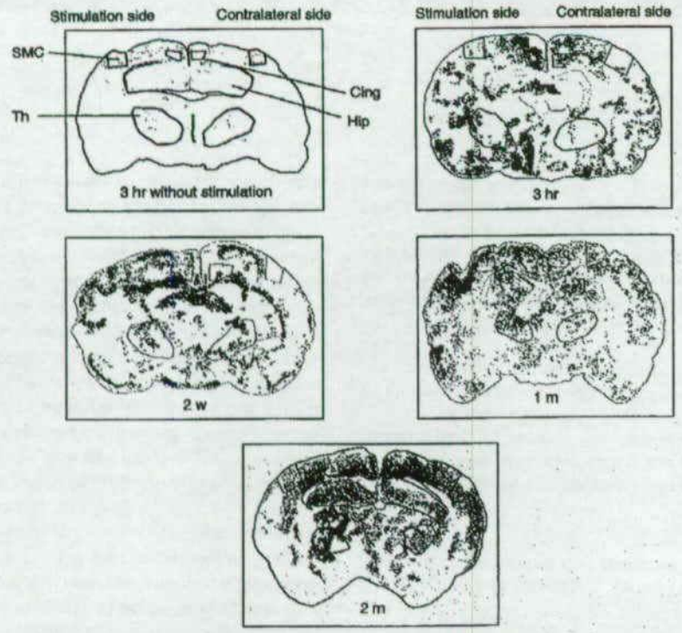

FIGURE 5. Distributions of *c-Fos*-immunopositive cells in coronal sections that contain the stimulation site after three hours without stimulation, and after three hours, two weeks, one month, and two months of stimulation. The dots indicate immunopositive cells on the ipsilateral and contralateral sides to the stimulation. The density of *c-Fos*-immunopositive cells changed gradually from three hours to two months. SMC, sensorimotor cortex; Th, thalamus; Cing, cingulate gyrus; Hip, hippocampus.

Figure 5 shows the distribution of *c-Fos*-immunopositive cells in coronal sections from a control animal and from rats after three hours, two weeks, and two months of stimulation. After three hours of stimulation, higher densities of *c-Fos*-immunopositive cells were found in the dentate gyrus, thalamus, and medial amygdala on the side ipsilateral to the electrical stimulation than in the same areas on the contralateral side. Immunopositivity also was observed in the piriform cortex, hippocampus, and striatum of both hemispheres. After two weeks of stimulation, higher densities of *c-Fos*-immunopositive cells were found in the neocortex, hippocampus, dentate gyrus, fimbria, corpus callosum, ventral premaxillary nucleus, and hypothalamus of both hemispheres. *c-Fos*-immunopositive cells also were noted in the reticular nucleus of the thalamus of the contralateral cerebrum. After one month of stimulation, higher densities of *c-Fos*-immunopositive cells were found in the neocortex, hippocampus, dentate gyrus, fimbria, and corpus callosum of both hemispheres, and in the thalamus of the contralateral hemisphere. After two months of stimulation, higher densities of *c-Fos*-immunopositive cells were found in the hippocampus, thalamus, and corpus callosum on both sides.

To evaluate the changes in *c-Fos* expression level in each hemisphere, we compared cell density between the ipsi- and contralateral sides. The *c-Fos*-immunopositive cell ratios for the contra- and ipsilateral sides of stimulation were calculated (Fig. 6). At the early stage, higher densities of *c-Fos*-immunopositive cells were observed in the sensorimotor cortex, cingulate gyrus, and thalamus on the stimulation side. However, *c-Fos* expression level began to increase slightly in the sensorimotor cortex on the opposite side after two weeks of stimulation. The expression of *c-Fos* in the sensorimotor cortex on the contralateral side after one month of stimulation was enhanced. At this point, *c-Fos* expression extended to the thalamic nucleus and cingulate cortex on both sides. After two months, a higher density of *c-Fos*-immunopositive cells was observed on the side contralateral to the stimulation.

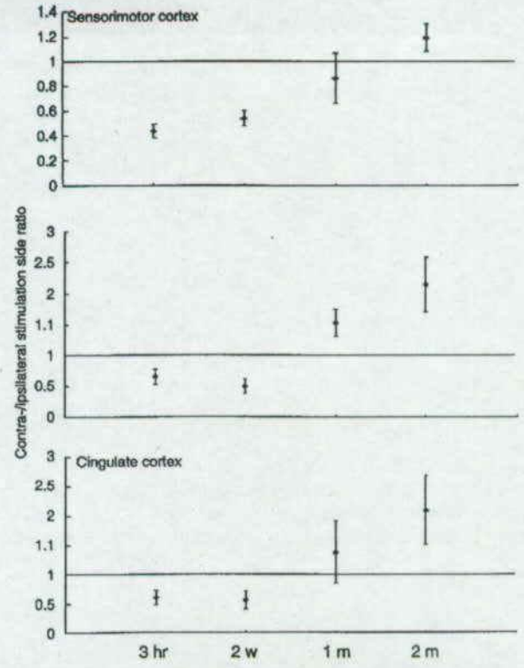

FIGURE 6. Cell densities on ipsilateral and contralateral sides compared in terms of positive cell ratios for contralateral/ipsilateral sides to stimulation in sensorimotor cortex (A), cingulate cortex (B), and thalamus (C). At the early stage, higher densities of *c-Fos*-immunopositive cells were observed on the stimulated side. However, after two months, higher densities of *c-Fos*-immunopositive cells were noted on the side contralateral to the stimulation.

Discussion

The use of chronic MCS as a treatment for medically refractory deafferentation pain, mainly thalamic pain, was initiated by Tsubokawa et al. and Katayama et al. (1,2). Katayama et al. reported excellent or good control of pain (pain reduction > 60%) in about 50% of patients employing this therapeutic technique for follow-up periods of more than two years (2). More recently, this procedure has been used as a treatment for movement disorders, including Parkinson's disease (13,14) and poststroke involuntary movement (15–17). Katayama et al. speculated that the therapeutic effects on involuntary movements are related to the desynchronization of abnormal activities that are transmitted to the corticospinal tract (17). Such an abnormal distribution of neural activity and the constitution of the neural network associated with the sensorimotor function could change in response to chronic MCS.

We examined the *c-Fos* expression after the long-term chronic electrical stimulation of the sensorimotor cortex in rats. It has been reported that epileptic seizures can induce high *c-Fos* expression levels in various areas of the brain in animals. Morgan et al. first described a marked and specific induction of *c-Fos* in an identifiable population of what *in vivo* following metrazol-induced seizures in mice (18). Doi et al. also found that electroconvulsive therapy induces a strong *c-Fos* expression in all regions of the brain except the thalamus (19).

In this study, the *c-Fos* expression induced by chronic sensorimotor cortex stimulation demonstrated the functional activation of several cortical and deep brain structures, mainly the sensorimotor cortex, thalamus, hippocampus, and cingulate gyrus. This pattern of *c-Fos* expression differed from that observed after epileptic seizures in previous studies (18,19). In addition, we observed no convulsions or seizurelike symptoms during chronic stimulation in any of our rats. Voskuyl et al. have described in detail the threshold of electrical stimulation that induces convulsions (20). According to their experimental study employing nonanesthetized rats, the conditions of approximately 1.3 μA with a 2-msec duration and a 50-Hz frequency represent the threshold for convulsions in rats. The stimulation parameters used in our study were a 0.12-msec duration, a 25-Hz frequency and an intensity that was 80% the threshold for muscle contraction (approximately 2–3 V). Thus, convulsive seizures could hardly have occurred during the chronic sensorimotor cortex stimulation in this study.

It also was confirmed that degenerating neurons are absent in the sensorimotor cortex immediately below the stimulation electrode, as determined by the FJB histochemical staining technique (12). The *c-Fos* expression observed in this study was therefore almost completely induced by the electrical stimulation of the sensorimotor cortex without the induction of epileptic seizures or neuronal degeneration.

Several experimental studies of the distribution of *c-Fos* expression after electrical or magnetic cortical stimulation have been conducted. Sagar et al. stimulated the rat sensorimotor cortex electrically and examined *c-Fos* expression immunohistochemically. Three hours after the start of stimulation, focal nuclear *c-Fos* staining was observed in the sensorimotor cortex and thalamus, pontine nucleus, globus pallidus, and cerebellum (21). Viltart and Sequeira also stimulated the rat sensorimotor cortex for one hour and observed catecholaminergic neuronal activity. Their data suggest that the stimulation of the sensorimotor cortex preferentially activates catecholaminergic neurons of the rostral ventrolateral medulla (22).

On the other hand, certain studies have shown experimental studies using transcranial magnetic stimulation (TMS). Hausmann et al. demonstrated a marked increase

in *c-Fos* expression level in neurons of the parietal cortex and in a few scattered neurons of the hippocampus of rats after chronic repetitive TMS for 14 days (23). According to an experimental study by Doi et al., six TMS sessions induce widespread nuclear *c-Fos*-like immunopositivities in the frontal cortex, lateral orbital cortex, striatum, lateral septal nucleus, piriform cortex, dentate gyrus, and Ammon's horn among other structures. These reactivities were greater than those for two TMS sessions (19). Various affected portions of the brain and patterns of *c-Fos* expression after cortical stimulation were noted in the above-mentioned studies. The results obtained basically agree with each other and with our results for short-term stimulation. However, *c-Fos* expression and its changes were monitored for only a short period in all the previous studies. Even in that using daily repetitive TMS, the maximum period of *c-Fos* expression observation was two weeks. To the best of out knowledge, this is the first experimental study in which *c-Fos* expression and its changes on sensorimotor cortex stimulation have been observed for two months.

The most important results obtained in this study can be summarized as follows:

1. *c-Fos* was significantly expressed immediately after the sensorimotor cortex stimulation as compared with that in the control.
2. Such *c-Fos* expression changed with time. It generally became extended over the cerebral cortex and deep brain structures with an increase in stimulation duration.
3. *c-Fos* expression was noted not only on the stimulation side, but also on the contralateral side. After two months, a higher density of *c-Fos*-immunopositive cells was observed on the side contralateral to the stimulation than on the stimulation side.

Animal and human research over the recent decades has provided increasing evidence of the brain's capacity for reorganizing its neural networks to adapt to environmental needs. From the basis of the results of this study, functional modulation as demonstrated by *c-Fos* expression suggests the existence of MCS-induced neural plasticity that intensifies with the stimulation duration.

The *c-Fos* expression after continuous cortical stimulation was noted not only on the side ipsilateral to the stimulation but also on the contralateral side. Several clinical observations appear to support this phenomenon. In our clinical experience, gradual improvements of gait have sometimes been observed after long-term MCS in patients with post-stroke motor deficit. Canavero and Bonicalzi reported the effects of bilateral MCS on plegic stroke rehabilitation. They stated that MCS can modestly boost the rehabilitation effects in chronic stroke patients, with effects differing between ipsilateral and contralateral stimulations (24). These findings appear to support the beneficial effects of long-term MCS of the contralateral cerebral hemisphere. Further research is needed to elucidate the mechanism underlying the predominant effect of the long-term stimulation of the contralateral side.

It has been speculated that the construction of an abnormal network in the upper central nervous system above a deafferentation site is associated with the mechanism of deafferentation pain onset (1,2,16). MCS could exert neuroplastic effects for coping with such an abnormal network. This characteristic of MCS, that is the induction of neural plasticity, may be useful for the application of MCS as a therapeutic method for other functional diseases. In fact, MCS is increasingly employed as a therapeutic method for various movement disorders and poststroke motor dysfunction. Its therapeutic indications should gradually expand owing to its unique ability to elicit neural plasticity.

Conclusions

Chronic sensorimotor cortex stimulation induced *c-Fos* expression, and the affected areas expanded, including the side contralateral to the stimulation, in association with stimulation duration. Such results indicate the existence of a high degree of neural plasticity in the brain induced by chronic sensorimotor cortex stimulation. Furthermore, on the basis of these results, it is speculated that chronic MCS modulates abnormal neural networks that develop in patients with deafferentation pain. This therapeutic method should be adopted as a treatment for various functional diseases involving with abnormal neural reconstruction.

Acknowledgment

This work was supported by a Grant-in-Aid for Scientific Research (A18209046 and C17591535) from the Ministry of Education, Culture, Sports, Science, and Technology of Japan.

Conflict of Interest

The authors reported no conflict of interest.

References

1. Tsubokawa T, Katayama Y, Yamamoto T, Hirayama T, Koyama S. Chronic motor cortex stimulation in patients with thalamic pain. *J Neurosurg* 1993;78:393–401.

2. Katayama Y, Fukaya C, Yamamoto T. Poststroke pain control by chronic motor cortex stimulation: neurological characteristics predicting a favorable response. *J Neurosurg* 1998;89:585–591.

3. Conner JM, Culberson A, Packowski C, Chiba AA, Tuszynski MH. Lesions of the basal forebrain cholinergic system impair task acquisition and abolish cortical plasticity associated with motor skill learning. *Neuron* 2003;38:819–829.

4. Kleim JA, Barbay S, Nudo RJ. Functional reorganization of the rat motor cortex following motor skill learning. *J Neurophysiol* 1998;80:3321–3325.

5. Nudo RJ, Wise BM, SiFuentes F, Milliken GW. Neural substrates for the effects of rehabilitative training on motor recovery after ischemic infarct. *Science* 1996;272:1791–1794.

6. Nudo RJ, Jenkins WM, Merzenich MM. Repetitive microstimulation alters the cortical representation of movements in adult rats. *Somatosens Mot Res* 1990;7:463–483.

7. Teskey GC, Monfils MH, VandenBerg PM, Kleim JA. Motor map expansion following repeated cortical and limbic seizures is related to synaptic potentiation. *Cereb Cortex* 2002;12:98–105.

8. Herrera DG, Robertson HA. Activation of *c-fos* in the brain. *Prog Neurobiol* 1996;50:83–107.

9. Reddington M, Priller J, Treichel J, Haas C, Kreutzberg GW. Astrocytes and microglia as potential targets for calcitonin gene related peptide in the central nervous system. *Can J Physiol Pharmacol* 1995;73:1047–1049.

10. Fujiki M, Steward O. High frequency transcranial magnetic stimulation mimics the effects of ECS in upregulating astroglial gene expression in the murine CNS. *Brain Res Mol Brain Res* 1997;44:301–308.

11. Ito D, Imai Y, Ohsawa K, Nakajima K, Fukuuchi Y, Kohsaka S. Microglia-specific localisation of a novel calcium birding protein, Iba1. *Brain Res Mol Brain Res* 1998;57:1–9.

12. Schmued LC, Albertson C, Slikker W Jr. Fluoro-Jade: a novel fluorochrome for the sensitive and reliable histochemical localization of neuronal degeneration. *Brain Res* 1997;751:37–46.

13. Canavero S, Bonicalzi V, Paolotti R et al. Therapeutic extradural cortical stimulation for movement disorders: a review. *Neurol Res* 2003;25:118–122.

14. Pagni CA, Altibrandi MG, Bentivoglio A et al. Extradural motor cortex stimulation (EMCS) for Parkinson's disease: history and first results by the Study Group of the Italian Neurosurgical Society. *Acta Neurochir Suppl* 2005;93:113–119.

15. Franzini A, Ferroli P, Leone M, Broggi G. Stimulation of the posterior hypothalamus for treatment of chronic intractable cluster headaches: first reported series. *Neurosurgery* 2003;52:1095–1099.

16. Katayama Y, Yamamoto T, Kobayashi K, Kasai M, Oshima H, Fukaya C. Motor cortex stimulation for post-stroke pain: comparison of spinal cord and thalamic stimulation. *Stereotact Funct Neurosurg* 2001;77:183–186.

17. Katayama Y, Yamamoto T, Kobayashi K, Oshima H, Fukaya C. Deep brain and motor cortex stimulation for post-stroke movement disorders and post-stroke pain. *Acta Neurochir Suppl* 2003;87:121–123.

18. Morgan JI, Cohen DR, Hempstead JL, Curran T. Mapping patterns of *c-fos* expression in the central nervous system after seizure. *Science* 1987;237:192–197.

19. Doi W, Sato D, Fukuzako H, Takigawa M. *c-Fos* expression in rat brain after repetitive transcranial magnetic stimulation. *Neuroreport* 2001;12:1307–1310.

20. Voskuyl RA, Dingemanse J, Danhof M. Determination of the threshold for convulsions by direct cortical stimulation. *Epilepsy Res* 1989;3:120–129.

21. Sagar SM, Sharp FR, Curran T. Expression of *c-fos* protein in brain: metabolic mapping at the cellular level. *Science* 1988;240:1328–1331.

22. Viltart O, Sequeira H. Induction of *c-fos*-like protein in bulbar catecholaminergic neurones by electrical stimulation of the sensorimotor cortex in the rat. *Neurosci Lett* 1999;260:65–68.

23. Hausmann A, Weis C, Marksteiner J, Hinterhuber H, Humpel C. Chronic repetitive transcranial magnetic stimulation enhances *c-fos* in the parietal cortex and hippocampus. *Brain Res Mol Brain Res* 2000;76:355–362.

24. Canavero S, Bonicalzi V. Transcranial magnetic stimulation for central pain. *Curr Pain Headache Rep* 2005;9:87–89.

Neuromodulation

Technology at the Neural Interface

VOLUME X • NUMBER 3 • JULY 2007

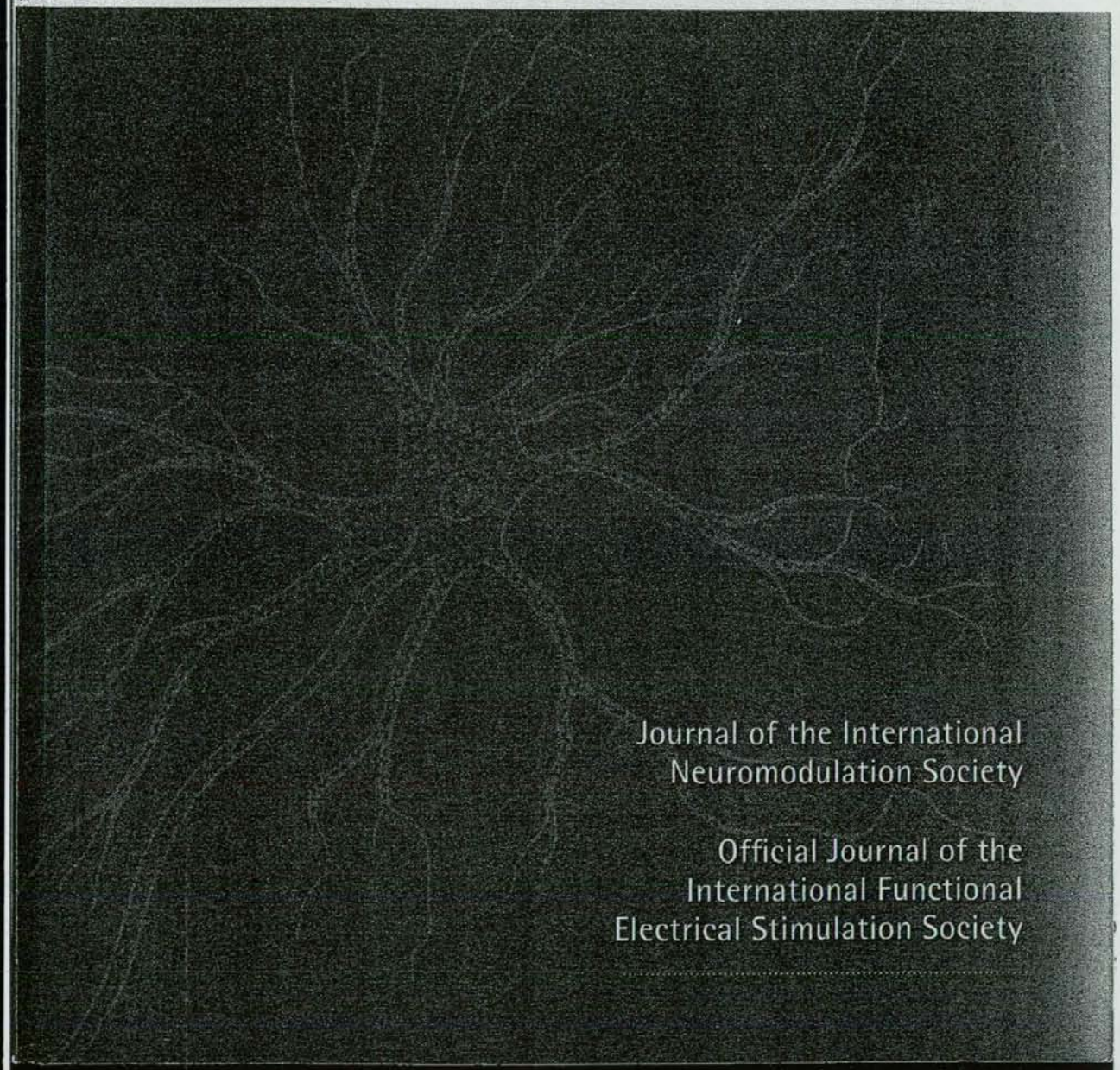

Journal of the International Neuromodulation Society

Official Journal of the International Functional Electrical Stimulation Society

NEUROMODULATION: TECHNOLOGY AT THE NEURAL INTERFACE

Volume 10 • Number 3 • 2007
http://www.blackwell-synergy.com/loi/ner

ORIGINAL ARTICLE

Changes in Glucose Metabolism in Cerebral Cortex and Cerebellum Correlate With Tremor and Rigidity Control by Subthalamic Nucleus Stimulation in Parkinson's Disease: A Positron Emission Tomography Study

Takafumi Nagaoka, MD, PhD • Yoichi Katayama, MD, PhD • Toshikazu Kano, MD, PhD • Kazutaka Kobayashi, MD, PhD • Hideki Oshima, MD, PhD • Chikashi Fukaya, MD, PhD • Takamitsu Yamamoto, MD, PhD

Department of Neurological Surgery, Division of Applied System Neuroscience, Nihon University School of Medicine, Tokyo, Japan

ABSTRACT

Objective. Employing [^{18}F]fluorodeoxyglucose (FDG) positron emission tomography (PET) to assess the correlation between the effect of deep brain stimulation (DBS) on the subthalamic nucleus (STN) and the regional cerebral metabolic rate of glucose (rCMRGlc) in advanced Parkinson's disease patients ($N=8$). **Materials and Methods.** On the basis of patients' diary records, we performed FDG-PET during the off-period of motor activity with on- or off-stimulation by STN-DBS on separate days and analyzed the correlation between changes in motor symptoms and alterations in the rCMRGlc. **Result.** When FDG-PET was performed, the motor score on the unified Parkinson's disease rating scale (UPDRS) was 64% lower with on-stimulation than with off-stimulation ($p < 0.001$, Wilcoxon single-rank test). STN-DBS increased the rCMRGlc in the posterior part of the right middle frontal gyrus, which corresponded to the premotor area, and the right anterior lobe of the cerebellum ($p < 0.005$, paired t-test). No region exhibited a decrease in rCMRGlc. Among the items of the UPDRS motor score, the changes in resting tremor and rigidity of the left extremities showed a significant correlation with the changes in rCMRGlc observed in the right premotor area ($p < 0.02$ and $p < 0.05$, respectively, Spearman's rank correlation). **Conclusions.** STN-DBS either activates the premotor area or normalizes the deactivation of the premotor area. These FDG-PET findings obtained are consistent with the idea that STN-DBS modifies the activities of neural circuits involved in motor control.

KEY WORDS: *Deep brain stimulation, FDG-PET, Parkinson's disease, subthalamic nucleus.*

Submitted: July 25, 2006; accepted: April 2, 2007. Address correspondence and reprint requests to: Takamitsu Yamamoto, MD, PhD, Department of Neurological Surgery, Nihon University School of Medicine, 30-1, Ohyaguchi, Kamimachi, Itabashi-ku, Tokyo 173-8610, JAPAN. Email: nusmyama@med.nihon-u.ac.jp

Introduction

Recent clinical studies have demonstrated that deep brain stimulation (DBS) of the subthalamic nucleus (STN) affords great benefits to the daily activities of patients with advanced Parkinson's disease (PD) (1–7), and lowers the requirement for levodopa (or an equivalent medication) (3,8). In most of these studies, the major effects of STN stimulation were observed during the off-period or off-medication (1–8).

The mechanism(s) underlying these neurologic improvements induced by STN-DBS has been investigated by positron emission tomography (PET) employing [^{15}O]H_2O or [^{18}F]fluorodeoxyglucose (FDG), reflecting regional cerebral activity. Previous PET studies (9–15) have demonstrated that STN-DBS increases activity of the supplementary motor area, the premotor area, the dorsolateral prefrontal cortex, or the anterior cingulate gyrus during the execution of motor tasks or at rest.

However, little is yet known concerning the relationship of changes in regional cerebral activity induced by STN-DBS to improvement of motor symptoms. In this study, we analyzed the correlation between changes in motor symptoms and alterations in the regional cerebral metabolic rate of glucose (rCMRGlc) using FDG-PET, which provides information on changes in the regional cerebral activity (16).

Clinical Materials and Methods

Patient Population and Protocol

This study was approved by the Institutional Review Board of Nihon University Hospital and Nishidai Clinic, and written consent was obtained from each subject after a detailed explanation of the procedures had been given. We studied eight patients with advanced idiopathic PD (four men and four women; mean age: 61.9 ± 11.1 years). The patients in this study were referred to us by neurologists specializing in the treatment of PD. The effects of various combinations of medical therapies were examined by the referring neurologists. All patients responded well to levodopa, but showed severe motor fluctuations. Using the Hoehn and Yahr disability scale to assess levels of disability, all patients were at Stages 3, 4, or 5 during off-periods and Stages 1, 2, or 2.5 during on-periods. In this article, we use "off-period" to indicate the bad period of daily fluctuations in motor symptoms and "on-period" to indicate the good period of daily fluctuation in motor symptoms.

There were two reasons why these patients had become disabled despite having adequate responses to levodopa:

1. Severe fluctuations in motor symptoms occurred, with or without levodopa-induced dyskinesia, in five cases.
2. Sufficient doses of levodopa-induced side-effects, which included nausea and vomiting, arrhythmia, orthostatic hypotension, and psychiatric symptoms, in three cases.

The dose of medication, expressed in this article, is the levodopa-equivalent dose (LED) (17) (the regular dose of levodopa plus carbidopa [or benserazide] + 0.75 × the dose of controlled-release levodopa plus carbidopa + 10 × the dose of bromocriptine + 100 × the dose of pergolide) and the total dose of monoamine oxidase B (MAO-B) inhibitor (selegiline).

Patient's Diary for Advanced PD

We employed a patient's diary to assess the patterns of motor fluctuations and the durations of the on- and off-periods over the whole day (Fig. 1). This diary included items for medication and motor symptoms. Motor function was evaluated according to a four-point rating scale: 1) almost normal; 2) moderately disabled; 3) markedly disabled; and 4) severely disabled. The patients evaluated these items and recorded the results by themselves at one-hour intervals. Based on this record, the on- and off-periods of daily fluctuations in motor symptoms were determined for each patient.

Surgical Procedures Performed

A Leksell series G head frame (Elekta Instruments AB, Stockholm, Sweden) was fixed to the

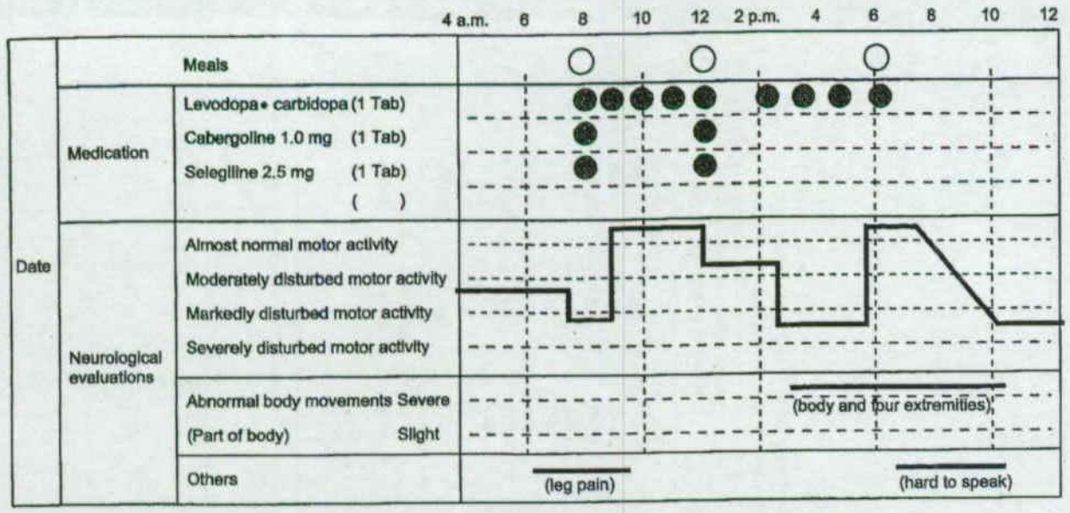

FIGURE 1. Patient's diary. Patients recorded their medication and motor function by themselves at one-hour intervals. This diary was used for estimating the patterns of motor fluctuations and the durations of the on- and off-periods.

skull. Magnetic resonance (MR) imaging was carried out at a 1-mm slice thickness, and the anterior commissure (AC) and posterior commissure (PC) were identified using specialized software (Leksell SurgiPlan, Elekta). An X-ray indicator also was employed to identify the AC and PC on plain X-ray photographs. Three-dimensional trajectories were evaluated with a digitized version of the Schaltenbrand–Wahren atlas (AtlasSpace, Elekta).

In an attempt to minimize cerebrospinal fluid leakage and, consequently, intraoperative brain shift, the head of each patient was elevated to approximately 30° from the horizontal plane and a burr hole was made 30–35 mm anterior to the coronal suture and 20–25 mm lateral to the midline. With such a burr hole placement, the electrode was oriented at angles of 40–50° to the horizontal plane of the AC-PC line and 5–10° to the sagittal plane in STN-DBS. This trajectory of the electrode was approximately parallel to the long axis of the STN and ran sequentially through the zona incerta and STN.

A tungsten semimicroelectrode (about 200–400 kohm), guided by an outer cannula (catheter insertion needle for a Leksell stereotactic system) was used for extracellular recording, and the location of the STN was identified electrophysiologically. A DBS lead (model 3387; Medtronic Inc., Minneapolis, MN, USA) with four contact points, numbered 0–3 sequentially from the most distal contact 0 to the most proximal contact 3, was placed in such a way that Contact 0 was located in the ventral portion of the STN and Contact 3 was located at Forel H2 or the zona incerta. Immediately after completion of the stereotactic operation, we performed MR imaging again with the stereotactic frame fixed to the skull, and the location of the electrode was confirmed. The placement of the DBS lead for both sides was carried out by single-stage surgery in all patients (4,18,19). After test stimulation for several days, each DBS lead was implanted and connected to implantable pulse generators (model 7426; Medtronic).

Stimulation Procedures

In our protocol for STN-DBS, stimulation was started by selecting Contact 0 or 1 as the cathode and Contact 3 as the anode, aiming to stimulate a wide area of the STN and supra-STN area. If such bipolar stimulation was insufficient for

alleviating neurologic symptoms, monopolar stimulation was then performed. At the time of PET examination, all patients had beneficial effects of their bipolar stimulation. The selected stimulation conditions at PET examination were such that Contact 0 or 1 was taken as the cathode and Contact 3 as the anode, with an intensity and frequency within the ranges of 1.6–2.7 V and 120–150 Hz, respectively; and the pulse width was 150 ms in all patients. On the basis of the stereotactic coordinates of the DBS leads, identified by postoperative MR imaging, the contacts used as the cathode were found to be located in the center or bottom of the STN, and the contacts used as the anode were located at Forel H2 or the zona incerta, just above the STN.

Positron Emission Tomography

To evaluate the effects of STN stimulation, a PET study was performed at approximately one month after surgery. FDG-PET was performed twice on two consecutive days. Before the day of the PET study, DBS was turned off, overnight, for at least 12 hours to create an identical situation for comparison of the effects of STN-DBS between on- and off-stimulation.

On the day of the PET study, DBS was turned on in the morning and left on during the daytime. PET was carried out in the afternoon during the off-period in each case and stimulation was turned off at night. On the next morning, stimulation was kept off during daytime, and PET was carried out in the afternoon during the off-period in each case. The patients were requested to maintain the dose and schedule of their medication stable during the study. They were evaluated using the unified Parkinson's disease rating scale (UPDRS) and Hoehn and Yahr disability scale immediately before and after the PET on each day, and the scores before and after the PET were averaged.

All patients fasted overnight prior to undergoing FDG-PET. During the PET study, each patient was positioned supine in the scanner with a three-dimensional laser alignment of the orbitomeatal line. All PET studies were performed in the three-dimensional mode using PosiCam-HZL (Positron Co., Houston, TX, USA). Two-dimensional image planes with 61 slices were used with an axial field of view of 16.6 cm and a transaxial resolution of 6.1 mm (full width half maximum) in all directions. All subjects underwent the PET study after injection of 350 MBq FDG, and each PET session (on- and off-stimulation) was performed at rest with the eyes closed and with a low ambient auditory noise.

Data Analysis

Differences between the motor score and subscores on the UPDRS during on-stimulation and off-stimulation (DBS off—DBS on) were used for analysis. A difference was considered significant if the p-value was 0.001 or less. Differences in regional FDG uptake level between on- and off-stimulation were analyzed by the paired t-test employing SPM99 software (Wellcome Department of Cognitive Neurology, London, UK), implemented in MATLAB (Mathworks, Sherborn, MA, USA). The scans from each subject were realigned and stereotactically normalized into the atlas of Talairach and Tournoux (20). Subsequently, the images were scaled proportionally and smoothed with an isotopic Gaussian kernel (full width half maximum 12 mm for all directions) to reduce for interindividual anatomical variability and to improve the signal-to-noise ratio. Changes in clusters were accepted as significant if the p-values corrected for multiple comparisons were 0.005 or less. Spearman's rank correlation was used to analyze the relationships between changes in subscores on the UPDRS and changes in rCMRGlc in each cluster. A correlation was considered significant if the p-value was 0.05 or less.

Results

Neurological Improvement Following STN-DBS

In comparison to off-stimulation, a marked neurologic improvement was observed during on-stimulation (Table 1). The UPDRS motor score during the off-period decreased from

TABLE 1. Patient Characteristics

Patient no./sex/age	Age at onset (year)	Dominantly affected side	Handedness	Hoehn and Yahr		UPDRS part III				Medication (mg/day)			
				On-period		On-period		Off-period		LED		MAO-B inhibitor	
				DBS-off	DBS-on	DBS-off	DBS-on	DBS-off	DBS-on	Pre op	Post op	Pre op	Post op
1/M/42	36	Left	Right	2	1	18	11	50	20	1300	650	10	5
2/M/63	53	Left	Right	2.5	0	42	11	49	11	710	500	0	0
3/F/71	55	Left	Right	2	1	21	21	34	24	300	200	0	0
4/M/76	43	Left	Right	2	0	28	24	35	31	445	445	2.5	2.5
5/F/50	48	Right	Right	1	0	11	2	26	6	330	330	0	0
6/M/68	58	Left	Right	2.5	1	13	1	36	6	1100	1100	5.0	5.0
7/F/63	58	Right	Right	1	0	16	0	23	0	713	713	0	0
8/F/62	49	Left	Right	2.5	0	13	14	51	10	770	770	0	0
Mean	50			1.94	0.4	20	11	38.0	14	708	588	2.2	1.6
SD	7.67			0.6	0.5	10	9.1	11	11	356	283	3.6	2.3
p-value				0.003†		0.032*		0.001‡		0.179		0.351	

*$p < 0.05$, Wilcoxon single-rank test.
†$p < 0.01$, Wilcoxon single-rank test.
‡$p < 0.001$, Wilcoxon single-rank test.
UPDRS part III, motor ratings on the unified Parkinson's disease rating scale; on- and off-periods, periods of best and worst motor activity in the daytime; LED, levodopa-equivalent dose; MAO-B, monoamine oxidase B; Pre op, before deep brain stimulation of the subthalamic nucleus (STN-DBS); Post op, at the time of [^{18}F]fluorodeoxyglucose-positron emission tomography (FDG-PET) examination.

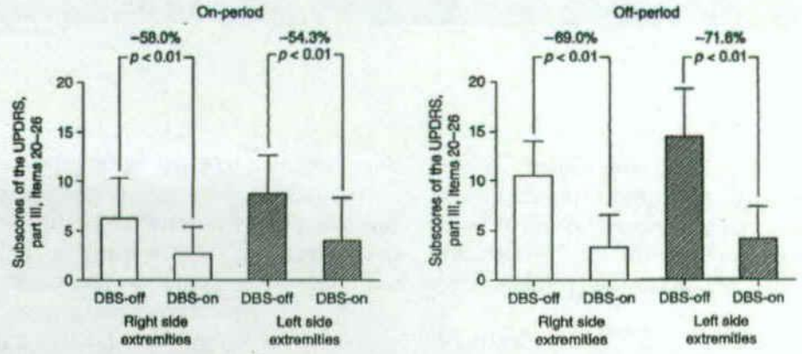

FIGURE 2. Effects of bilateral STN-DBS on the UPDRS motor score (subscores of the UPDRS, part III, items 20–26) as compared between the right and left extremities. Statistical significance was determined by Wilcoxon single-rank test. STN-DBS, deep brain stimulation of the subthalamic nucleus; UPDRS, unified Parkinson's disease rating scale.

38.0 ± 10.9 to 13.5 ± 10.5 ($p < 0.001$), and the mean Hoehn and Yahr disability scale during the off-period decreased from 3.88 ± 0.64 to 1.50 ± 0.89 ($p < 0.001$).

All eight patients were right hand dominant cases. The UPDRS motor score of the left side extremities (subscores of the UPDRS, part III, items 20–26), during the off-period, decreased from 14.50 ± 4.81 to 3.88 ± 3.04 ($p < 0.01$) following bilateral STN-DBS. The UPDRS motor score of the right side extremities (subscores of the UPDRS, part III, items 20–26), during off-period, also decreased from 10.50 ± 3.55 to 3.25 ± 3.33 following bilateral STN-DBS ($p < 0.01$) (Fig. 2). When comparing medication use after surgery to medication use before surgery, the LED during the PET study decreased from 708.4 ± 355.9 to 588.4 ± 282.8 mg/day, and the dose of MAO-B inhibitor decreased from 2.19 ± 3.64 to 1.56 ± 2.29 mg/day (Table 1). Because three out of eight patients in the present study did not take sufficient doses of levodopa, even before surgery, due to unbearable side-effects, no significant decreases were noted during the PET study in terms of either the LED or dose of MAO-B inhibitor.

Changes in rCMRGlc Induced by STN-DBS

Compared to the situation with that during off-stimulation, extended clusters of increased rCMRGlc were observed during on-stimulation in the right middle frontal gyrus corresponding to the premotor area (BA 6; $x = 24$, $y = 2$, $z = 58$; and $x = 16$, $y = -6$, $z = 58$), and in the right anterior lobe of the cerebellum ($x = 14$, $y = -44$, $z = -14$; Table 2). No similar changes in rCMRGlc were found in either the left middle frontal gyrus or the left anterior lobe of the cerebellum. There were no clusters of significantly decreased rCMRGlc seen (Fig. 3).

Relationship of Motor Symptoms to rCMRGlc

Among the items of the UPDRS motor score, resting tremor of the left extremity ($r^2 = 0.828$, $p < 0.02$) and rigidity of the left extremity ($r^2 = 0.368$, $p < 0.05$) showed clear correlations with changes seen in rCMRGlc in the right

TABLE 2. Brain Regions With a Significantly Altered rCMRGlc on FDG-PET During Bilateral STN-DBS, Ordered According to Their Peak Z-scores

Region	Talairach coordinates			Z_{max}	Voxels per cluster
	x	y	z		
Increased rCMRGlc					
Right middle frontal gyrus	24	2	58	4.02	185
	16	−6	58	3.7	
Right rostral cerebellar lobe	14	−44	−14	3.53	103

Peak activations ($p < 0.001$, > 32 voxels) in the left-right (*x*), anterior-posterior (*y*), and superior-inferior (*z*) planes (20). rCMRGlc, regional cerebral metabolic rate of glucose.

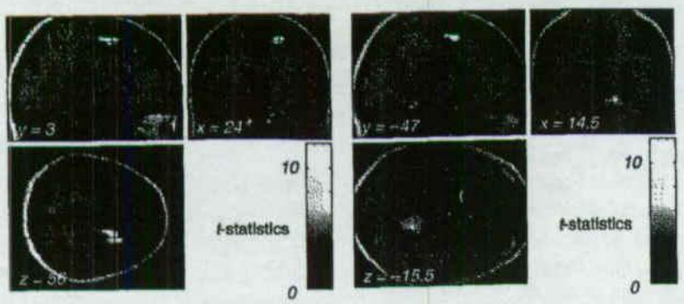

FIGURE 3. Regions associated with significant changes in rCMRGlc (DBS on—DBS off) as measured with SPM99 ($p < 0.005$ for cluster level corrected for multiple comparisons; color bars represent *t*-values). The figure shows transverse, sagittal, and coronal views in projection onto brain slices of a standard MRI (x/y/z coordinates according to the atlas of Talairach and Tournoux). rCMRGlc, Regional cerebral metabolic rate of glucose; MRI, magnetic resonance imaging; PD, Parkinson's disease; DBS, deep brain stimulation.

premotor area, but not with that in the right anterior cerebellum. Other items of the UPDRS motor score, such as speech, facial expression, resting tremor of the head and neck, action or postural tremor of the hands, rigidity of the neck, motor performance of the hands and legs, arising from a chair, posture, gait, postural stability, and body bradykinesia and hypokinesia, revealed no significant correlations with changes seen in rCMRGlc, in either the right premotor area or the right anterior cerebellum (Table 3).

Discussion

Changes in Cerebral Activity Induced by STN-DBS

In this study, changes in rCMRGlc were detected

TABLE 3. Correlations Between Unified Parkinson's Disease Rating Scale (UPDRS) Subscores and Changes of Regional Cerebral Metabolic Rate of Glucose (rCMRGlc) in the Right Premotor Area and Right Rostral Cerebellum

UPDRS part III subcategories		Changes of UPDRS scores (DBS_{on}–DBS_{off})	*p*-values: Right premotor area	*p*-values: Right rostral cerebellum
18. Speech		−1.309 ± 0.463	0.7686	0.4925
19. Facial expression		−1.356 ± 0.479	0.8455	0.3805
20. Tremor at rest	face and neck	−0.250 ± 0.463	0.0956	0.505
	left	−1.125 ± 0.398	0.0156*	0.3775
	right	−1.250 ± 0.366	–	0.0722
21. Action or postural tremor of hands	left	−0.750 ± 0.707	0.4687	0.945
	right	−0.625 ± 0.744	–	0.0728
22. Rigidity	neck	−1.125 ± 0.835	0.2301	0.9203
	left	−2.625 ± 1.188	0.0462*	0.819
	right	−1.625 ± 1.302	–	0.601
23+24+25+26 (finger taps, hand movements, alternating movements of hands, and leg agility)	left	−4.750 ± 3.495	0.1859	0.1658
	right	−3.750 ± 2.816	–	0.7528
27. Arising from a chair		−0.875 ± 1.126	0.6123	0.8925
28. Posture		−1.000 ± 1.069	0.2083	0.0851
29. Gait		−1.250 ± 1.165	0.5403	0.5403
30. Postural stability		−1.500 ± 1.309	0.3775	0.7438
31. Body bradykinesia and hypokinesia		−1.625 ± 0.916	0.1876	0.5209
Total score on UPDRS part III		−25.250 ± 14.130	0.1939	0.447

*$p < 0.05$, Spearman's rank correlation test. DBS, deep brain stimulation.

in the premotor area (BA6) and the anterior lobe of the cerebellum. Previous PET studies (9–15) have demonstrated various areas, such as the supplementary motor area, premotor area, dorsolateral prefrontal cortex, and anterior cingulate gyrus (11,13,14,21), activated or deactivated by STN-DBS.

One obvious cause of variability in the results of PET studies is differences in study design. Changes in cerebral activity may be dependent on the nature of the tasks employed during these PET studies. In the present study, FDG-PET was performed at rest without the execution of motor tasks. The observed changes in rCMRGlc can thus be related to motor symptoms at rest. For example, changes related to postural tremor may not be detected using such a study design. Consistent with our findings, Limousin et al. (11) reported that when the effect of STN-DBS at rest is examined, reqional cerebral blood flow undergoes increases in the sensorimotor (BA 4) and premotor (BA 6) areas.

Another possible cause of the variability in results of PET studies may be differences in location of the DBS leads. In previous PET investigations, the location of the DBS leads has not always been specified in detail. We implanted DBS leads with a sagittal plane angle of approximately 45° with reference to the AC–PC line. All of our patients preferred stimulation of the STN together with areas just above the STN (4).

Clinical observations have shown that stimulation of areas just above the STN can produce a marked attenuation of tremor, rigidity, and levodopa-induced dyskinesia. Anatomical studies have demonstrated that many pathways that are involved in motor control, such as cerebellothalamic, pallidothalamic, and pallidosubthalamic fibers, pass through these areas. Future PET studies need to analyze the relationship between the locations of the DBS leads and activated or deactivated areas.

Correlation of Motor Symptoms With Activity of the Premotor Area

Previous PET studies have not included detailed examinations of the relationships between improvements of the symptoms and activated or deactivated areas. The present findings indicated that the rCMRGlc of the right prefrontal area increased in association with attenuation of resting tremor and rigidity of the left extremities.

Although the STN was stimulated bilaterally, a strong lateralization of the stimulation-induced changes was observed on the right side. The most probable explanation for such lateralization was the predominance of symptoms on the left side in the patients included in this study: six out of eight patients demonstrated predominant symptoms on the left side (Table 1). This could have led to a greater chance of detecting changes in rCMRGlc on the right side and their correlation to an improvement of symptoms on the left side. Such an inference implies that changes in activity of the premotor area are closely related to tremor at rest on the contralateral side.

Mechanisms of Changes in rCMRGlc

The efferents of the STN mediate information to the premotor area via pallidothalamic and thalamocortical fibers, whereas the cerebellar afferents project predominantly to the primary motor area via thalamocortical fibers (19,22–24). It is possible that STN-DBS may activate the premotor area through pallidothalamic and thalamocortical fibers. Another possibility is that changes in the activity of the premotor area are the result, rather than the cause, of attenuation of resting tremor and rigidity. According to recent human imaging studies, the premotor area plays an important role in spatial attention and memory (25,26), or the planning and execution of voluntary movements (27–29). Simon et al. (24) demonstrated, in a functional MR imaging study, that motor preparation is mainly related to the caudal portion of the premotor area, whereas the more rostral portion is involved in spatial attention and memory. It appears possible, therefore, that the activity of the premotor area is deactivated in patients with resting tremor and rigidity, which would presumably disturb the appropriate processing of motor

preparation, and such deactivation becomes normalized when these symptoms are controlled by STN-DBS. If this inference is in fact correct, the observed increase in rCMRGlc in the present study could represent a normalization of the deactivation, rather than a direct activation, of the premotor area.

The effects of STN-DBS on changes in activity of the cerebellum remain controversial. Hilker et al. (30) reported that the rCMRGlc in the anterior cerebellum is decreased by STN-DBS. In contrast, Vafaee et al. (15) observed an increase in regional cerebral metabolic rate of oxygen consumption in the cerebellum during STN-DBS. The activation of the anterior lobe of the cerebellum detected in this study could be accounted for by antidromic activation of the cerebellothalamic fibers passing through the areas just above the STN (31) (vida supra). The detailed relationships between the location of the DBS leads and activation of the anterior lobe of the cerebellum need to be determined in future studies.

Conclusions

The present data suggest that STN-DBS normalizes deactivation of the premotor area in association with control of resting tremor and rigidity of the contralateral extremities. Such an inference, in turn, implies that resting tremor and rigidity may disturb appropriate processing of motor preparation within the premotor area in patients with PD. These FDG-PET findings are consistent with the idea that STN-DBS modifies the activities of neural circuits involved in motor control.

Acknowledgments

This work was supported by Grants-in-Aid for Scientific Research from the Ministry of Education, Culture, Sports, Science and Technology, Japan (nos. A12307029 and A15209047), by grants from the Ministry of Education, Culture, Sports, Science and Technology for the promotion of industry–university collaboration at Nihon University, and a program grant from the Ministry of Health, Labor and Welfare, Japan.

References

1. Benabid AL, Pollak P, Gross C et al. Acute and long-term effect of subthalamic nucleus stimulation in Parkinson's disease. *Stereotact Funct Neurosurg* 1994;62:76–84.

2. Brown RG, Dowsey PL, Brown P et al. Impact of deep brain stimulation on upper limb akinesia in Parkinson's disease. *Ann Neurol* 1999;45:473–488.

3. Burchiel KJ, Anderson VC, Favre J et al. Comparison of pallidal and subthalamic nucleus deep brain stimulation for advanced Parkinson's disease: results of a randomized, blind pilot study. *Neurosurgery* 1999;45:1375–1382.

4. Katayama Y, Kasai M, Oshima H et al. Subthalamic nucleus stimulation for Parkinson disease: benefits observed in levodopa-intolerant patients. *J Neurosurg* 2001;95:213–221.

5. Krack P, Batir A, Van Blercom N et al. Five-year follow-up of bilateral stimulation of the subthalamic nucleus in advanced Parkinson's disease. *N Eng J Med* 2003;349:1925–1934.

6. Kumar R, Lozano AM, Sime E et al. Comparative effects of unilateral and bilateral subthalamic nucleus deep brain stimulation. *Neurology* 1999;53:561–566.

7. Limousin P, Krack P, Pollak P et al. Electrical stimulation of the subthalamic nucleus in advanced Parkinson's disease. *N Eng J Med* 1998;339:1105–1111.

8. Moro E, Scerrati M, Romito LMA et al. Chronic subthalamic nucleus stimulation reduces medication requirements in Parkinson's disease. *Neurology* 1999;53:85–90.

9. Antonini A, Landi A, Benti R et al. Functional neuroimaging (PET and SPECT) in the selection and assessment of patients with Parkinson's disease undergoing deep brain stimulation. *J Neurosurg Sci* 2003;47:40–46.

10. Brooks DJ, Samuel M. The effects of surgical treatment of Parkinson's disease on brain function: PET findings. *Neurology* 2000;55 (12 Suppl. 6):S52–S59.

11. Limousin P, Krack P, Pollak P et al. Changes in cerebral activity pattern due to subthalamic nucleus or internal pallidum stimulation in Parkinson's disease. *Ann Neurol* 1997;43:283–291.

12. Sestini S, Scotto di Luzio A, Ammannati F et al. Changes in regional cerebral blood flow caused by deep-brain stimulation on the subthalamic nucleus in Parkinson's disease. *J Nucl Med* 2002;43:725–732.

13. Strafella AP, Sadikot AF, Dagher A. Subthalamic deep brain stimulation does not induce striatal dopamine release in Parkinson's disease. *NeuroReport* 2003;14:1287–1289.

14. Thobois S, Dominey P, Fraix V et al. Effects of subthalamic nucleus stimulation on actual and imagined movement in Parkinson's disease: a PET study. *J Neurol* 2002;249:1689–1698.

15. Vafaee MS, Ostergaard K, Sunde N et al. Focal changes of oxygen consumption in cerebral cortex of patients with Parkinson's disease during subthalamic stimulation. *NeuroImage* 2004;22:966–974.

16. Raichle ME, Gusnard DA. Appraising the brain's energy budget. *Proc Natl Acad Sci USA* 2002;99:10237–10239.

17. The Deep-brain Stimulation for Parkinson's Disease Study Group. Deep-brain stimulation of the subthalamic nucleus or the pars interna of the globus pallidus in Parkinson's disease. *N Engl J Med* 2001;345:956–963.

18. Yamamoto T, Katayama Y, Fukaya C et al. New method of deep brain stimulation therapy with two electrodes implanted in parallel and side by side. *J Neurosurg* 2001;95:1075–1078.

19. Yamamoto T, Katayama Y, Kano T et al. Deep brain stimulation for the treatment of parkinsonian, essential, and post-stroke tremor: suitable stimulation method and changes of effective stimulation intensity. *J Neurosurg* 2004;101:201–209.

20. Talairach J, Tournoux P. *Co-planar stereotactic atlas of the human brain: 3-dimension proportional system: an approach to cerebral imaging*. Stuttgart, Germany: George Thieme Verlag, 1988.

21. Ceballos-Baumann AO, Boecker H, Bartenstein P et al. A positron emission tomographic study of subthalamic nucleus stimulation in Parkinson's disease: enhanced movement-related activity of motor association cortex and decreased motor cortex resting activity. *Arch Neurol* 1992;56:997–1003.

22. Lehericy S, Grand S, Pollak P et al. Clinical characteristics and topography of lesions in movement disorders due to thalamic lesions. *Neurology* 2001;57:1055–1066.

23. Star PA, Vitek JL, Bakay RAE. Deep brain stimulation for movement disorders. *Neurosurg Clin N Am* 1998;9:381–402.

24. Simon SR, Meunier M, Piettre L et al. Spatial attention and memory versus motor preparation: premotor cortex involvement as revealed by fMRI. *J Neurophysiol* 2002;88:2047–2057.

25. Courtney SM, Petit L, Maisog JM et al. An area specialized for spatial working memory in human frontal cortex. *Science* 1998;279:1347–1351.

26. Stern CE, Owen AM, Tracey I et al. Activity in ventrolateral and mid-dorsolateral prefrontal cortex during nonspatial visual working memory processing: evidence from functional magnetic resonance imaging. *NeuroImage* 2000;11:392–399.

27. Deiber MP, Ibanez V, Sadato N et al. Cerebral structures participating in motor preparation in humans: a positron emission tomography study. *J Neurophysiol* 1996;75:233–247.

28. Grafton ST, Fagg AH, Arbib MA et al. Dorsal premotor cortex and conditional movement selection: a PET functional mapping study. *J Neurophysiol* 1998;79:1092–1097.

29. Van Oostende S, Van Hecke P, Sunaert S et al. FMRI studies of the supplementary motor area and the premotor cortex. *NeuroImage* 1997;6:181–190.

30. Hilker R, Voges J, Weisenbach S et al. Subthalamic nucleus stimulation restores glucose metabolism in associative and limbic cortices and in cerebellum: evidence from a FDG-PET study in advanced parkinson's disease. *J Cereb Blood Flow Metab* 2004;24:7–16.

31. Naus CG, Flumerfelt BA, Hrycyshyn AW. Topographic specificity of aberrant cerebellorubral projections following neonatal hemicerebellectomy in the rat. *Brain Res* 1984;20:1–15.

Neuromodulation

Technology at the Neural Interface

VOLUME XI • NUMBER 4 • NOVEMBER 2008

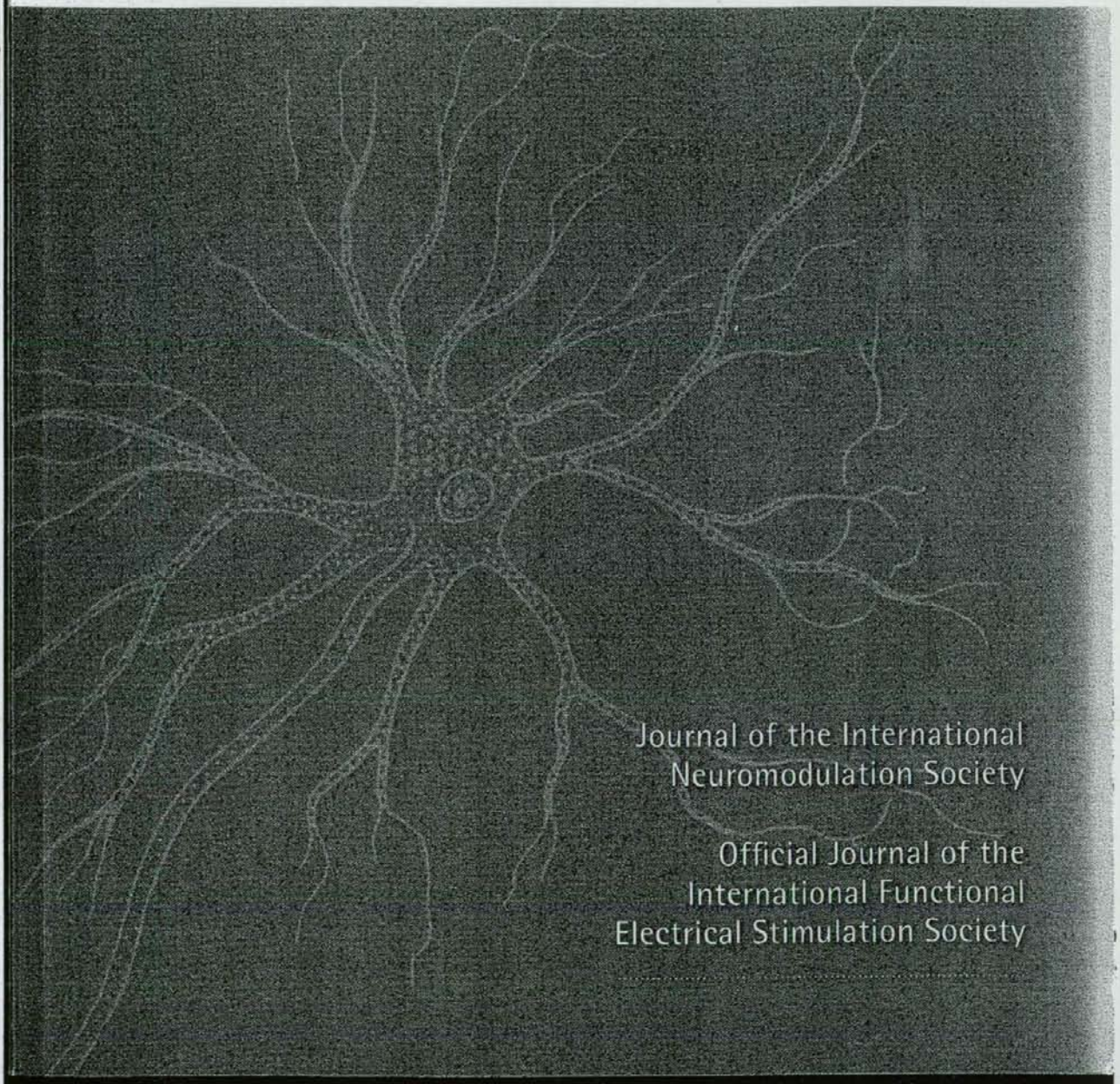

Journal of the International Neuromodulation Society

Official Journal of the International Functional Electrical Stimulation Society

Volume 11 • Number 4 • 2008
http://www.blackwell-synergy.com/loi/ner

ORIGINAL ARTICLE

Direction and Predictive Factors for the Shift of Brain Structure During Deep Brain Stimulation Electrode Implantation for Advanced Parkinson's Disease

Toshiki Obuchi, MD* • Yoichi Katayama, MD, PhD*† • Kazutaka Kobayashi, MD, PhD*† • Hideki Oshima, MD, PhD* • Chikashi Fukaya, MD, PhD*† • Takamitsu Yamamoto, MD, PhD*†

Department of Neurological Surgery and Division of Applied System Neuroscience, †Department of Advanced Medical Science, Nihon University School of Medicine, Tokyo, Japan

ABSTRACT

Objectives. The aims of this study were to clarify the direction and degree of brain shift, and to determine the predictive factors for a brain shift during deep brain stimulation (DBS) of the subthalamic nucleus (STN). **Materials and Methods.** To evaluate the brain shift during bilateral STN-DBS, the position of the anterior commissure (AC), posterior commissure (PC), midcommissure point (MC), and tip of the frontal lobe and anterior horn of the lateral ventricle were calculated pre- and poststereotactic operations in the three-dimensional direction employing special software (Leksell SurgiPlan). To determine the predictive factors for a brain shift, patient's age, operation hours, width of the third ventricle, bicaudate index (BCI), and cella media index (CMI) were compared with the shift of MC. **Results.** In 50 patients, the MC shifted mainly in the posterior direction (*y*-axis: 1.27 ± 0.7 mm), and the shifts in the inferior direction (*z*-axis: 0.11 ± 0.43 mm) and lateral direction (*x*-axis: 0.02 ± 0.39 mm) were small. The shift of the MC in the posterior direction correlated well with the shift of the tip of the anterior lobe and anterior horn. Among the predictive factors examined, namely, the patient's age, operation hours, width of the third ventricle, BCI, and CMI, only the CMI showed a correlation with the shift of the MC ($r = 0.42$, $p < 0.01$, Pearson's correlation coefficient; and $p < 0.05$, logistic regression analysis). **Conclusions.** In bilateral STN-DBS, brain shift occurred mainly in the posterior direction, and the CMI is useful for the prediction of a brain shift. Enlargement of the body part of the lateral ventricle is the most reliable factor for predicting a brain shift.

KEY WORDS: *Brain shift, deep brain stimulation, Parkinson's disease, stereotactic operation, STN-DBS.*

Introduction

The recent marked increase in a number of patients who undergo deep brain stimulation (DBS), especially subthalamic nucleus (STN)-DBS, reflects the efficacy of this therapy (1–5), and accuracy of electrode placement is required for success of this therapy (6–9). Brain shift occurs after the skull and dura have been opened during the stereotactic operation, and this brain shift decreases the accuracy of target coordination calculated on the basis of preoperative magnetic resonance imaging (MRI) carried out when the skull is closed. An intraoperative brain shift is caused mainly by the outflow of cerebrospinal fluid (CSF) and by the influx of air into the intracranial space. Such intracranial air influx is caused not only by the CSF outflow, but also by a decreased intracranial blood volume.

Therefore, we fixed the angle of head elevation and the location of the burr hole during the STN-DBS procedure, and examined the MR images obtained before and immediately after implantation of the DBS electrode to compare the shift of brain structures occurring during the stereotactic operation.

In the present study, we attempted to clarify the direction and degree of brain shift during the stereotactic operation. In addition, we also attempted to determine the predictive factors for a brain shift that were recognizable before the stereotactic operation.

Submitted: October 23, 2007; accepted: February 20, 2008. Address correspondence and reprint requests to: Takamitsu Yamamoto, MD, PhD, Division of Applied System Neuroscience, Department of Advanced Medical Science, Nihon University School of Medicine, 30-1 Ohyaguchi Kamimachi, Itabashi-ku, Tokyo 173-8610, JAPAN. Email: nusmyama@med.nihon-u.ac.jp

Materials and Methods

Patient Population

Fifty patients (100 sides) with advanced Parkinson's disease treated by bilateral STN-DBS participated in this study. DBS was performed with the informed consent of each patient and family. The 50 patients consisted of 23 men and 27 women. The age range was from 44 to 76 years old, and the mean age was 63.5 ± 6.6 years old.

Surgical Procedures

After the patient had received a local anesthetic, a Leksell Series G head frame (Elekta Instrument AB, Stockholm, Sweden) was fixed to the skull. With the MRI indicator attached to the stereotactic head frame, MR imaging was carried out at a 1-mm slice thickness, and the anterior commissure (AC) and posterior commissure (PC) were identified with special software (Leksell SurgiPlan, Elekta Instrument AB) (Fig. 1). Fixing the head elevation at between 25 and 30 degrees from the horizontal plane of the ground surface and under local anesthesia, a dual-floor burr hole (15 mm in diameter) (10) was created 30 to 35 mm anterior to the coronal suture and 20 to 25 mm lateral to the midline.

The right side was always operated on first, but the burr hole was made bilaterally at first during the planning of the first trajectory. The dura was kept intact, and the burr hole was stuffed with a cotton sheet soaked in saline. After removing the right-side cotton sheet, the dura of the right burr hole was opened and the arachnoid membrane and cortical surface also were coagulated at the point of electrode insertion. The dura of the left-side burr hole was opened after a permanent DBS electrode (model 387; Medtronic Inc., Minneapolis, MN, USA) was implanted and fixed to the skull with the burr-hole ring and burr-hole cap included in the package of the DBS electrode.

The target was then approached from the burr hole at an angle of from 40 to 50 degrees to the horizontal plane of the AC–PC line (Fig. 2). Three-dimensional trajectory visualization and a digitized version of the Schaltenbrand–Wahren atlas (AtlasSpace, Elekta Instrument AB) were employed to confirm the structure through which the electrode passed (11). A microelectrode guided by an outer cannula was inserted into the STN region through a frontal burr hole to confirm the location of the STN, and a permanent DBS electrode for STN-DBS was implanted. A one-time bilateral operation was the choice of all patients. After finishing the bilateral electrode implantation, the first operation was completed. An implantable pulse generator was implanted under the anterior chest wall, and connected to the DBS electrode on a separate day under general anesthesia.

Calculation of the Shift of Brain Structures

Immediately after completion of the stereotactic operation and without implantable pulse generator implantation, we examined the MR images obtained again, while the sterotactic frame was still fixed to the skull and the MRI indicator was attached to the head frame. The location of the DBS electrode was confirmed on the SurgiPlan, and the difference between the pre- and postoperative coordinates of the AC, PC, midcommissure (MC), and tip of the frontal lobe and anterior horn was calculated as the index of brain shift. We also calculated the width of the third ventricle, bicaudate index (BCI; distance between the caudate nuclei divided by the maximum width between the frontal horns of the lateral ventricles), and cella media index (CMI; minimum width between the lateral ventricles at the cella media level divided by the cranial width at the same level) using the SurgiPlan before the operation (Fig. 3). To determine the predictive factors for a brain shift, we examined the correlation of patient's age, operation hours, width of the third ventricle, BCI, and CMI with the shift of the MC in the three-dimensional direction.

Statistical Analysis

Statistical analyses were performed using Pearson's correlation coefficient and logistic regression analysis. In this article, values for groups are expressed as the means ± standard deviation.

Results

Shift of the Frontal Lobe, Anterior Horn, and MC

The right side was always operated on first, and the location of the STN was investigated and identified by microelectrode recording. Once the right-side location of the STN had been identified by the microelectrode recording, the left-side identification of the STN by microelectrode

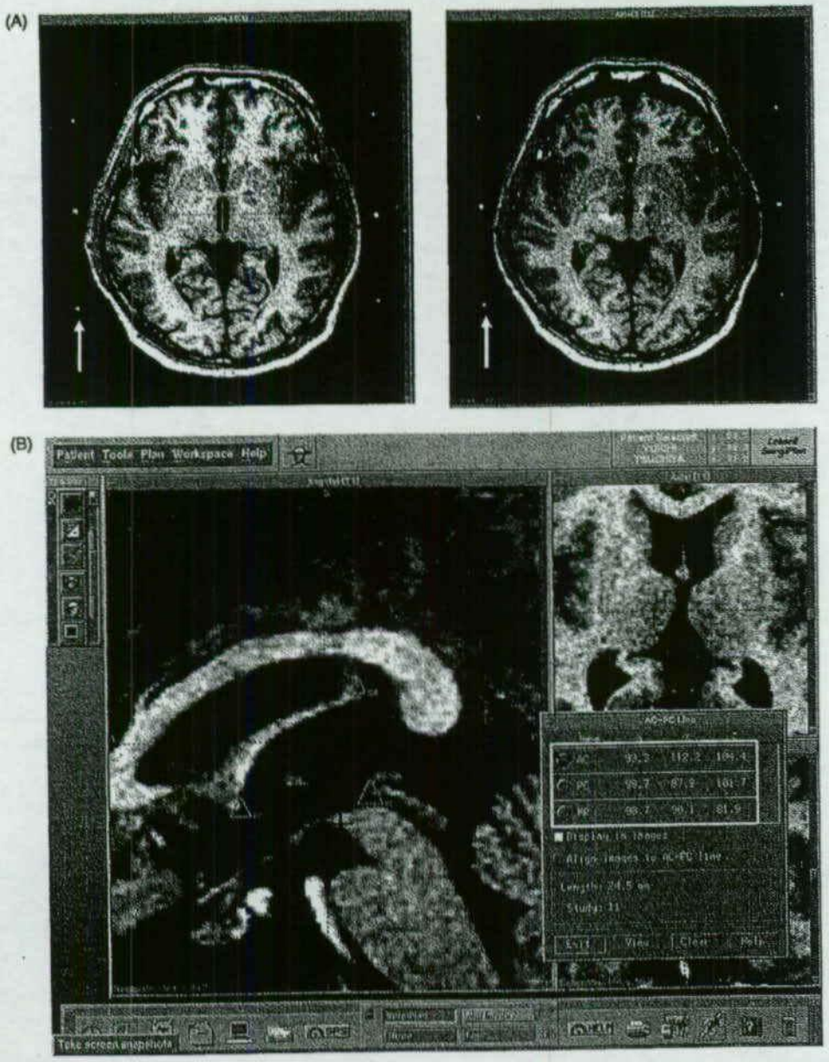

FIGURE 1. Comparison of the shift of midline structures employing SurgiPlan. (A) MRI indicator, which has six point markers (arrow), is fixed to the stereotactic head frame, and MRI data were transferred to SurgiPlan. The three-dimensional coordinates of the anterior commissure (AC), posterior commissure (PC), and midcommissure (MC) were compared between pre- and poststereotactic operations. On a postoperative MR imaging (right), an artifact of the deep brain stimulation electrode implanted into the subthalamic nucleus region can be observed. Green triangles indicate the points of AC and PC. (B) AC and PC (Green triangles) are identified on the sagittal plane of SurgiPlan. Three-dimensional coordinates of AC and PC were calculated using SurgiPlan (yellow rectangular area).

recording was easy and yielded almost the same three-dimensional coordinates as for the right side. The cortical surface sank during the microelectrode mapping and DBS electrode placement. Comparison of the pre- and postoperative MR images obtained in the spinal position revealed that the tip of the frontal lobe shifted mainly in the posterior direction (5.47 ± 2.22 mm on the right side and 5.13 ± 2.19 mm on the left side). The tip of the

TABLE 1. Brain Shift of Each Landmark Calculated Between Pre- and Poststereotactic Operations

	Shift (mm)					
	X (right–left)		*Y* (anterior–posterior)		*Z* (superior–inferior)	
	Mean ± SD	Maximum	Mean ± SD	Maximum	Mean ± SD	Maximum
Tip of right frontal lobe	2.20 ± 3.98	12.00	−5.47 ± 2.22	−10.10	0.63 ± 6.91	−19.80
Tip of left frontal lobe	−1.14 ± 2.99	−10.7	−5.13 ± 2.19	−11.70	0.69 ± 5.81	17.20
Tip of right anterior horn	0.54 ± 1.09	3.70	−3.69 ± 1.88	−8.70	0.63 ± 1.29	3.60
Tip of left anterior horn	−0.65 ± 1.22	−4.80	−3.26 ± 1.94	−8.10	0.63 ± 1.12	3.9
Midcommissure	−0.02 ± 0.39	−1.20	−1.27 ± 070	−3.45	−0.11 ± 0.43	1.00

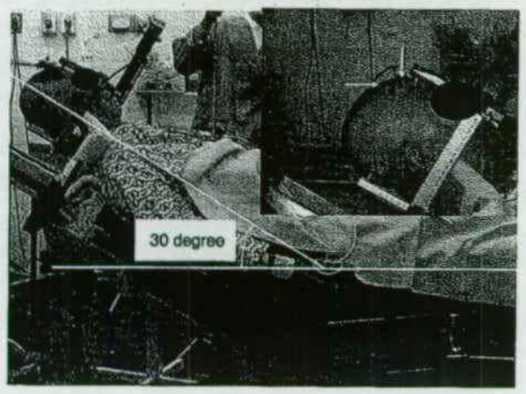

FIGURE 2. Head elevation and location of burr hole during the stereotactic operation. Head elevation is restricted to be under 30 degrees, and the burr hole (vertical arrow) is located 30 to 35 mm anterior to the bregma (horizontal arrow).

anterior horn also shifted mainly in the posterior direction (3.67 ± 1.88 mm on the right side and 3.26 mm on the left side). The MC also shifted mainly in the posterior direction (*y*-axis: 1.27 ± 0.7 mm), and the shifts in the inferior direction (*z*-axis: 0.11 ± 0.43 mm) and lateral direction (*x*-axis: 0.02 ± 0.39 mm) were small (Table 1).

The shift of the MC in each patient was plotted in the axial and sagittal planes (Fig. 4). The shift of the MC in the posterior direction correlated with the shift of the tip of the anterior lobe ($r = -0.59$ on the right side, $r = -0.50$ on the left side; Pearson's correlation coefficient) and with that of the tip of the anterior horn ($r = -0.63$ at the right, $r = -0.68$ at the left; Pearson's correlation coefficient) (Fig. 5).

Predictive Factors for Brain Shift

We examined the correlation of the postoperative shift of the MC in the posterior direction with the width of the third ventricle, BCI, CMI, age, and operation hours. Among these factors, only the CMI revealed a correlation with the shift of the MC ($r = 0.42$, $p < 0.01$; Pearson's correlation coefficient) (Fig. 6). Depending on the extent of the shift of the MC in the posterior direction, the patients were classified into two groups: one showing a shift of more than 1.5 mm ($N = 16$) and the other showing a shift of less than 1.5 mm ($N = 34$). Logistic regression analysis for these two groups suggested that the two groups demonstrated a significant difference in their CMI only ($p = 0.0157$) (Table 2).

Discussion

In the present study, the head elevation was fixed at between 25 and 30 degrees, and the burr hole was made 30 to 35 mm anterior to the bregma. This procedure enabled us to create the burr hole at the highest position on the cranium during the stereotactic operation and to reduce the overflow of CSF from the burr hole (1,11,12). Moreover, the trajectory of the electrode from this burr-hole point allowed passage through the STN over the longest distance. In the condition of cranial opening, when we elevated the head over 30 degrees, the inflow of air into the intracranial space increased with decrease in the volume of intracranial venous blood. We have not employed tissue sealants such as fibrin glue during the operation, and the space of the burr hole around the outer cannula

TABLE 2. Logistic Regression Analysis of the Posterior Shift of Midcommissure for Two Groups Showing Shifts Over 1.5 mm and Under 1.5 mm

	OR	95% CI	*p*-value
Age	0.965	0.86–1.082	0.54
Third ventricle	0.834	0.518–1.344	0.4562
Bicaudate index	0.831	0.587–1.177	0.2968
Cella media index	1.67	1.102–2.532	0.0157
Time	0.994	0.980–1.009	0.4484

95% CI: 95% confidence intervals; OR, odds ratio.

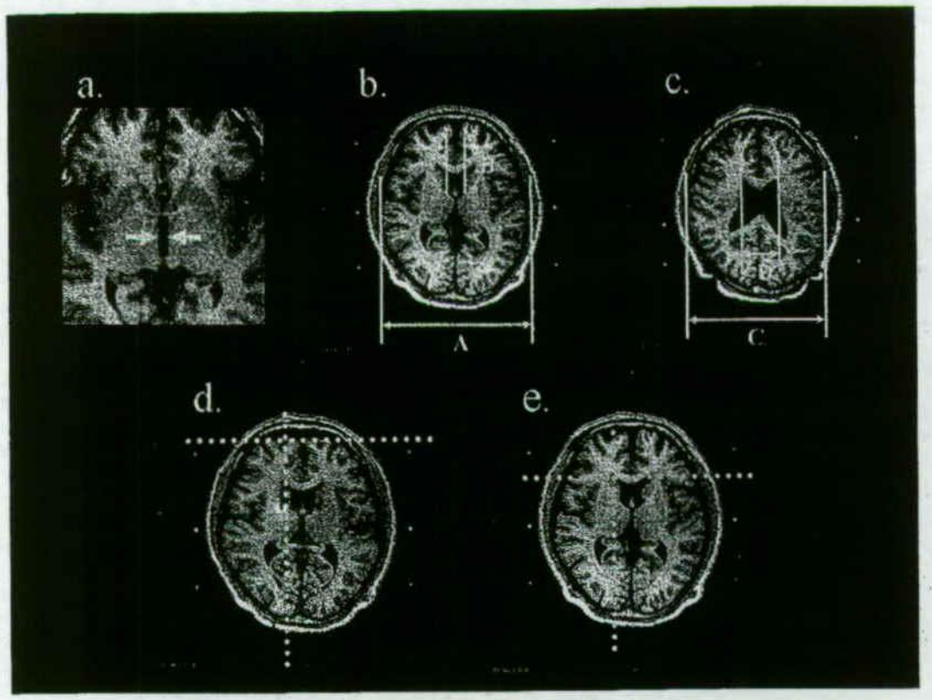

FIGURE 3. Calculation method and calculation points on SurgiPlan. (a) Width of the third ventricle. (b) Bicaudate index (BCI): B/A. (c) Cella media index (CMI): D/C. (d) Tip of the frontal lobe: Three-dimensional coordinates of cross points were compared between pre- and postoperation. (e) Tip of the anterior horn of the lateral ventricle: Three-dimensional coordinates of cross points were compared between pre- and postoperation.

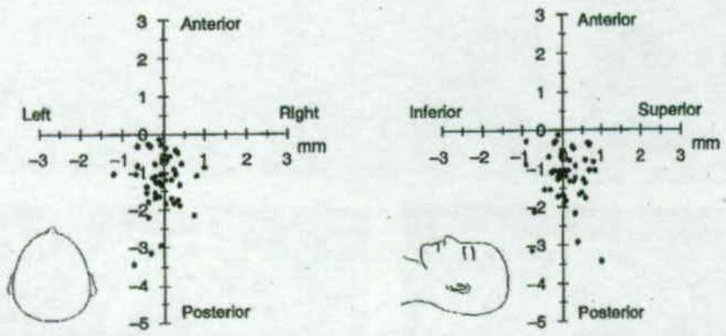

FIGURE 4. Shift of midcommissure (MC). Three-dimensional coordinate of MC (each dot), calculated immediately after the operation, was compared with the coordinate of MC calculated before the operation (cross point of each axis). Left indicates the axial plane, and right indicates the sagittal plane.

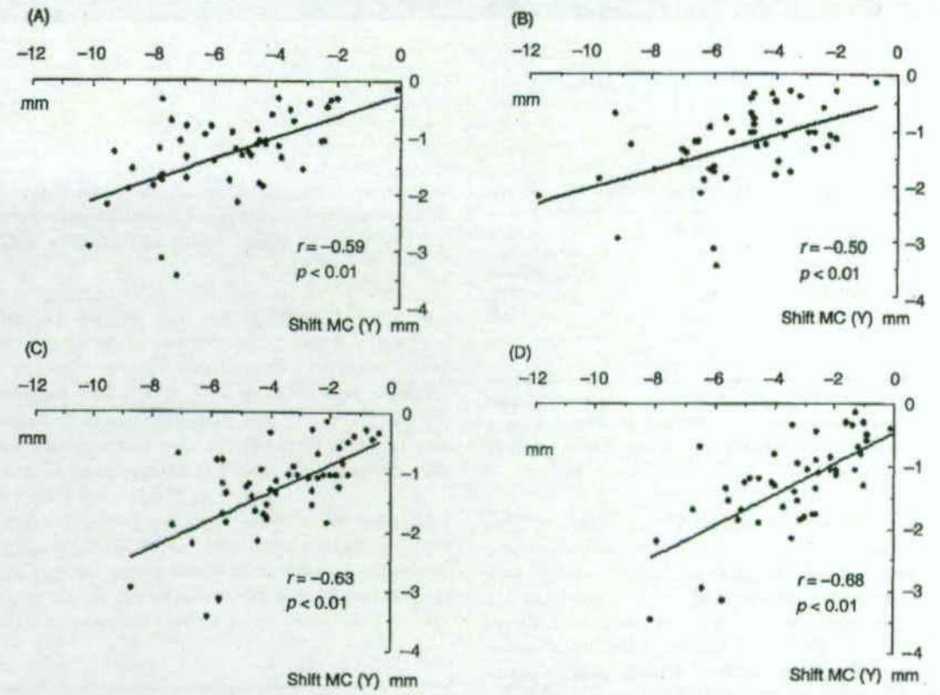

FIGURE 5. Comparison between the posterior shift of midcommissure (MC) and the tip of frontal lobe and anterior horn of the lateral ventricle. (A) Tip of right frontal lobe. (B) Tip of left frontal lobe. (C) Tip of right anterior horn. (D) Tip of left anterior horn.

for the microelectrode recording was stuffed with a cotton sheet soaked in saline. We used SurgiPlan to evaluate the three-dimensional coordinates of the brain structures, and the MC was selected as the indicator of brain shift, because the MC is located in the center of the midline structures and the AC and PC are accurate indicators for the stereotactic coordinates. As compared with the shift of the cortical surface, the shift of the MC was small and the width of the third ventricle demonstrated no significant change in our study.

Wester and Krakenes (13) have described results for stereotactic thalamotomy performed in the sitting position, and concluded that the brain mainly shifted vertically. They calculated the extent to which the cortical surface sank during the stereotactic operation, and concluded that the brain shift at the thalamic level should be estimated at about one-half of the extent of the operative sinking of the cortical surface. Pollo et al. (14) made a 3-mm twist drill hole for STN-DBS, and the dura mater was opened such that the diameter of the opening did not exceed that of their guiding tubes to prevent CSF leakage. They examined the location of the DBS electrode after the stereotactic operation, and the distances between the electrode and the expected and actual targets in the x- and y-axes were found to be 1.34 ± 1.02 mm and 1.03 ± 0.76 mm, respectively. In the z-axis, 39.7% of the stimulation contact points were located proximal to the target, and they concluded that the caudal brain shift depends on the head position and may occur during the implantation procedure. Winkler et al. (15) applied deformity analysis to pre- and postoperative three-dimensional MR images, and found that the brain shift occurred mainly in the posterior direction. The surface of the frontal cortical brain shifted 13 mm, and the region of the subthalamic nucleus revealed a 2-mm shift. In our study, in which the head elevation was restricted to under 30 degrees, the shift of the MC was mainly in the posterior direction, and the shifts in the lateral and inferior directions were small. Subdural air was always detected in the frontal subdural space.

Star et al. (9) reported that 19 (25%) of their 76 STN-DBS procedures showed a change of 2 mm or greater in the lateral or anteroposterior direction, and these changes did not appear to be associated with any particular age group, brain size, or degree of brain atrophy. We examined

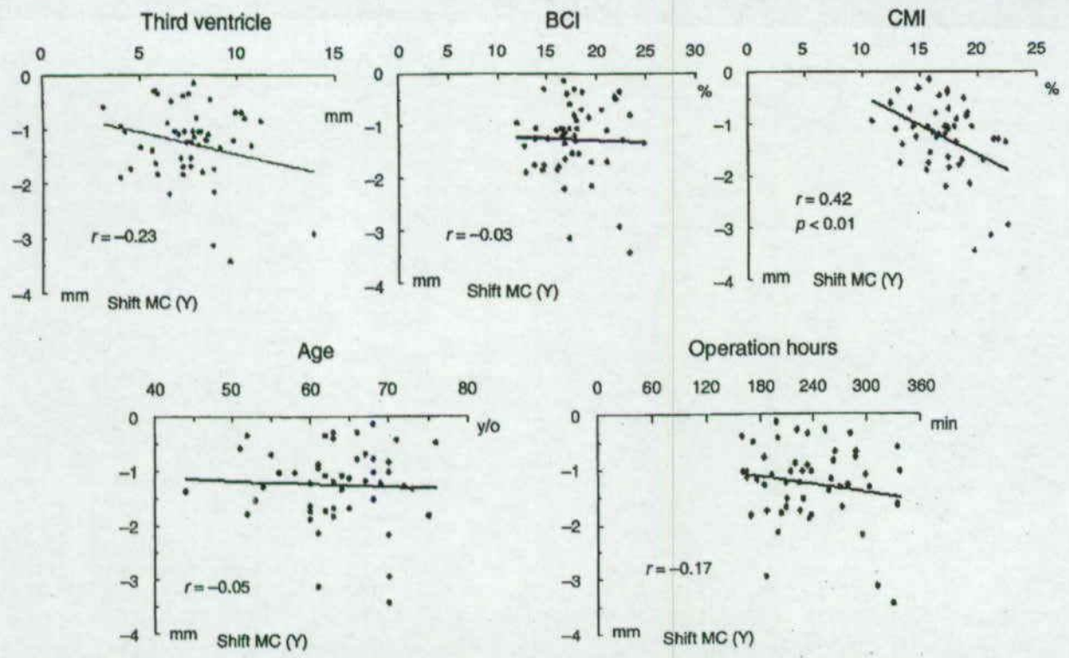

FIGURE 6. Comparison between the posterior shift of midcommissure (MC) and predicting factors for brain shift. Third ventricle, width of the third ventricle; BCI, bicaudate index; CMI, cella media index; age, patient's age; operation hours, from start of drilling the burr hole to the completion of deep brain stimulation electrode implantation.

the correlation of the shift of the MC with the width of the third ventricle, BCI, CMI, age, and operation hours. Among these items, only the CMI demonstrated a significant correlation with the shift of the MC. In our study, 16 of the 50 STN-DBS cases revealed a more than 1.5-mm brain shift in the posterior direction. Logistic regression analysis of the two different groups indicated that both groups showed a significant difference in CMI only. The width of the third ventricle and BCI demonstrated no significant differences. The BCI represents the anterior part of the lateral ventricle, but the CMI represents the body part of the lateral ventricle. Our findings suggest that the enlargement of the body part of the lateral ventricle, which represents the actual enlargement of the lateral ventricle, is the most reliable factor predicting an intraoperative brain shift.

There are several factors which can account for differences between the initial and intraoperative final targets: These include MR image distortion (16), brain shift (13,15) caused by CSF leakage and air influx, the neurophysiologic method (17–22) of finding the best target, and technical error. Zonenshayn et al. (23) reported that the average distance error between the final physiologic targets and the MRI-derived target was 2.6 ± 1.3 mm. Andrade-Souza et al. (24) reported that the mean distances between the optimal contact position and the planned target were 3.19 ± 1.19 mm using the red nucleus-based method, 3.42 ± 1.34 mm using indirect targeting, and 4.66 ± 1.33 mm using a modified direct targeting. These differences between the optimal contact position and the planned target involve not only brain shifts but also other factors as described above. We evaluated the differences in pre- and postoperative MC locations on three-dimensional MR images, and this difference in MC location proved useful for evaluating the brain shift itself during the stereotactic operation.

Once the location of the STN at the first side was identified by microelectrode recording and the chronic DBS electrode was implanted, the second side targeting of the STN was found to be almost the same as that of the first side in the present study. This result indicates that the difference in shift of the STN in the posterior direction is small between the first and second operated sides when our operation method is employed, including the head position, location of the burr hole, and early bilateral

burr-hole formation with an intact dura. We have implanted unilateral chronic DBS electrodes by the same operation method in 12 cases which included dystonia, tremor, and Parkinson's disease. In these 12 cases, the shift of the MC in the posterior direction was 0.87 ± 0.87 mm. The shift of the MC to the posterior direction after the bilateral chronic DBS electrode implantation in this study was 1.27 ± 0.70 mm, and the difference of MC shift in the posterior direction as compared with the unilateral DBS electrode implantation with our method was thus only 0.40 mm.

In order to determine the brain shift in real time during the stereotactic operation, the use of intraoperative ultrasound and intraoperative MR imaging is considered promising. If the correlation of the brain shift between the STN and cortical surface or anterior horn is examined as in this study, intraoperative estimation of the brain shift of the cortical surface or anterior horn by intraoperative ultrasound or intraoperative MR imaging can be used as a method of real-time monitoring. In addition, direct targeting of the STN which can identify the whole shape of the STN employing intraoperative MR imaging may prove to be an ideal method in the future.

Conclusion

We utilized the same conditions for head elevation and burr-hole location in STN-DBS for cases of advanced Parkinson's disease, and compared the pre- and postoperative MR images employing SurgiPlan. The shift of the MC was mainly in the posterior direction, and the most reliable predictive factor for a brain shift was the CMI, which is helpful for evaluating the enlargement of the body part of the lateral ventricle. Determinations of the shift direction and predictive factors for a brain shift are useful for achieving accurate targeting during stereotactic surgery.

Acknowledgments

The present work was supported by grants from the Ministry of Education, Culture, Sports, Sciences and Technology of Japan (Grants No. A-15209047 and No. C-18591614) and a grant for the promotion of industry–university collaboration at Nihon University.

Conflict of Interest

The authors reported no conflict of interest.

References

1. Katayama Y, Kasai M, Oshima H et al. Subthalamic nucleus stimulation for Parkinson's disease: benefits observed in levodopa-intolerant patients. *J Neurosurg* 2001;95:213–221.

2. Krack P, Batir A, Van Blercom N et al. Five-year follow-up of bilateral stimulation of the subthalamic nucleus in advanced Parkinson's disease. *N Engl J Med* 2003;349:1925–1934.

3. Lanotte MM, Rizzone M, Bergamasco B, Faccani G, Melcarne A, Lopiano L. Deep brain stimulation of the subthalamic nucleus: anatomical, neurophysiological, and outcome correlations with the effects of stimulation. *J Neurol Neurosurg Psychiatry* 2002;72:53–58.

4. Limousin P, Krack P, Pollak P et al. Electrical stimulation of the subthalamic nucleus in advanced Parkinson's disease. *N Engl J Med* 1998;339:1105–1111.

5. The Deep-Brain Stimulation for Parkinson's Disease Study Group. Deep-brain stimulation of the subthalamic nucleus or the pars interna of the globus pallidus in Parkinson's disease. *N Engl J Med* 2001;345:956–963.

6. Priori A, Egidi M, Pesenti A et al. Do intraoperative microrecordings improve subthalamic nucleus targeting in stereotactic neurosurgery for Parkinson's disease? *J Neurosurg Sci* 2003;47:56–60.

7. Rodriguez-Oroz MC, Rodriguez M, Guridi J et al. The subthalamic nucleus in Parkinson's disease: somatotopic organization and physiological characteristics. *Brain* 2001;124:1777–1790.

8. Romanelli P, Heit G, Hill BC et al. Microelectrode recording revealing a somatotopic body map in the subthalamic nucleus in humans with Parkinson's disease. *J Neurosurg* 2004;100:611–618.

9. Starr PA, Christine CW, Theodosopoulos PV et al. Implantation of deep brain stimulators into the subthalamic nucleus: technical approach and magnetic resonance imaging-verified lead locations. *J Neurosurg* 2002;97:370–387.

10. Yamamoto T, Katayama Y, Kobayashi K, Oshima H, Fukaya C. Dual-floor burr hole adjusted to burr-hole ring and cap for implantation of stimulation electrodes. *J Neurosurg* 2003;99:783–784.

11. Yamamoto T, Katayama Y, Kano T, Kobayashi K, Oshima H, Fukaya C. Deep brain stimulation for the treatment of parkinsonian, essential, and poststroke tremor: a suitable stimulation method and changes in effective stimulation intensity. *J Neurosurg* 2004;101:201–209.

12. Yamamoto T, Katayama Y, Fukaya C, Oshima H, Kasai M, Kobayashi K. New method of deep brain stimulation therapy with two electrodes implanted in parallel and side by side. *J Neurosurg* 2001;95:1075–1078.

13. Wester K, Krakenes J. Vertical displacement of the brain and the target area during open stereotaxic neurosurgery. *Acta Neurochirur (Wien)* 2001;143:603–606.

14. Pollo C, Vingerhoets F, Pralong E et al. Localization of electrodes in the subthalamic nucleus on magnetic resonance imaging. *J Neurosurg* 2007;106:36–44.

15. Winkler D, Tittgemeyer M, Schwarz J et al. The first evaluation of brain shift during functional neurosurgery by deformation field analysis. *J Neurol Neurosurg Psychiatry* 2005;76:1161–1163.

16. Bourgeois G, Magnin M, Morel A et al. Accuracy of MRI-guided stereotactic thalamic functional neurosurgery. *Neurosurgery* 1999;41:636–645.

17. Hamid NA, Mitchell RD, Mocroft P, Westby GW, Milner J, Pall H. Targeting the subthalamic nucleus for deep brain stimulation: technical approach and fusion of pre- and postoperative MR images to define accuracy of lead placement. *J Neurol Neurosurg Psychiatry* 2005;76:409–414.

18. Hutchison WD, Allan RJ, Opitz H et al. Neurophysiological identification of the subthalamic nucleus in surgery for Parkinson's disease. *Ann Neurol* 1998;44:622–628.

19. Lopez-Flores G, Miguel-Morales J, Teijeiro-Amador J et al. Anatomic and neurophysiological methods for the targeting and lesioning of the subthalamic nucleus: Cuban experience and review. *Neurosurgery* 2003;52:817–830.

20. Starr PA, Vitek JL, DeLong M, Bakay RA. Magnetic resonance imaging-based stereotactic localization of the globus pallidus and subthalamic nucleus. *Neurosurgery* 1999;44:303–313.

21. Sterio D, Zonenshayn M, Mogilner AY et al. Neurophysiological refinement of subthalamic nucleus targeting. *Neurosurgery* 2002;50:58–67.

22. Yokoyama T, Sugiyama K, Nishizawa S et al. Neural activity of the subthalamic nucleus in Parkinson's disease patients. *Acta Neurochir (Wien)* 1998;140:1287–1290.

23. Zonenshayn M, Rezai AR, Mogilner AY, Beric A, Sterio D, Kelly PJ. Comparison of anatomic and neurophysiological methods for subthalamic nucleus targeting. *Neurosurgery* 2000;47:282–292.

24. Andrade-Souza YM, Schwalb JM, Hamani C et al. Comparison of three methods of targeting the subthalamic nucleus for chronic stimulation in Parkinson's disease. *Neurosurgery* 2005;56(2 Suppl.):360–368.

NEUROMODULATION: TECHNOLOGY AT THE NEURAL INTERFACE

Volume 11 • Number 4 • 2008
http://www.blackwell-synergy.com/loi/ner

ORIGINAL ARTICLE

Intrathecal Drug Delivery Device Infection and Meningitis due to *Mycobacterium Fortuitum*: A Case Report

Hamidreza Aliabadi, MD • Richard K. Osenbach, MD

Division of Neurosurgery, Duke University Medical Center, Durham, NC, USA

ABSTRACT

Intrathecal drug delivery device infection with *Mycobacterium fortuitum* has not been reported previously. We report a case of an implanted baclofen pump infection and associated mycobacterium meningitis due to *Mycobacterium fortuitum*. The entire pump system was removed and the patient was treated successfully with a prolonged regimen of antibiotics.

KEY WORDS: *Baclofen pump infection, intrathecal drug delivery device, meningitis,* Mycobacterium fortuitum.

Introduction

Baclofen is a muscle relaxant, antispastic agent, and γ-aminobutyric acid agonist that acts at the spinal cord level to inhibit the release of excitatory neurotransmitters (eg, glutamate, aspartate) by inhibiting Ca^{2+} influx into presynaptic terminal. Baclofen may be administered directly into the intrathecal space. Doing so allows for much smaller drug doses to achieve therapeutic effects compared with oral administration, which had bioequivalent doses may be associated with an increased incidence of side-effects.

Intrathecal baclofen therapy using programmable implantable pumps is widely acknowledged to be clinically effective in the treatment of intractable spasticity of either spinal or cerebral origin by reducing muscle tone and spasm (1–3). However, implantation of such intrathecal drug delivery devices (IDDD) is associated with complications (4). Such complications include skin breakdown and infection at the pump implantation site, meningitis, cerebrospinal fluid leak, or mechanical problems such as catheter kinking or break.

Intrathecal drug delivery device infection is reported to occur in 1–2% of cases (4). These infections are usually due to organisms of low virulence. The organisms most implicated in shunt infections are the coagulase-negative staphylococci, such as *Staphylococcus epidermidis* which accounts for 50–75% of infections. The next most frequent causes of infection include *Staphylococcus aureus*, Gram-negative enteric bacteria, and anaerobic diphtheroids.

Case Report

A 60-year-old man with a history of an incomplete cervical spinal cord injury from a fall presented with progressively worsening spasticity. He presented to the Duke University Medical Center with significant quadriparesis and he was started on intravenous methylprednisolone. Computed tomography (CT) of his cervical spine revealed severe central canal stenosis at C5–6 due to degenerative disease as well as moderate central canal stenosis at C4–5 and C6–7 secondary to central disc protrusions and focal osteophyte at C7 but no acute fractures. CT of his thoracic

Submitted: October 10, 2007; accepted: February 20, 2008. Address correspondence and reprint requests to: Hamidreza Aliabadi, MD, Division of Neurosurgery, Duke University Medical Center, 13108 Rose Garden Lane, Durham, NC 27707, USA. Email: hamid.aliabadi@duke.edu

Reprinted from

Journal of Neurosurgery

Thalamic deep brain stimulation for writer's cramp

CHIKASHI FUKAYA, M.D., PH.D., YOICHI KATAYAMA, M.D., PH.D., TOSHIKAZU KANO, M.D., PH.D., TAKAFUMI NAGAOKA, M.D., PH.D., KAZUTAKA KOBAYASHI, M.D., PH.D., HIDEKI OSHIMA, M.D., PH.D., AND TAKAMITSU YAMAMOTO, M.D., PH.D.

NOVEMBER 2007 Volume 107, Number 5:977-982

American Association of Neurological Surgeons

WWW.THEJNS.ORG

J Neurosurg 107:977–982, 2007

Thalamic deep brain stimulation for writer's cramp

Chikashi Fukaya, M.D., Ph.D., Yoichi Katayama, M.D., Ph.D., Toshikazu Kano, M.D., Ph.D., Takafumi Nagaoka, M.D., Ph.D., Kazutaka Kobayashi, M.D., Ph.D., Hideki Oshima, M.D., Ph.D., and Takamitsu Yamamoto, M.D., Ph.D.

Department of Neurological Surgery, Nihon University School of Medicine; Division of Applied System Neuroscience, Graduate School of Medical Science, Tokyo, Japan

Object. Writer's cramp is a type of idiopathic focal hand dystonia characterized by muscle cramps that accompany execution of the writing task specifically. In this report, the authors describe the clinical outcome after thalamic deep brain stimulation (DBS) therapy in patients with writer's cramp and present an illustrative case with which they compare the effects of pallidal and thalamic stimulation. In addition to these results for the clinical effectiveness, they also examine the best point and pattern for therapeutic stimulation of the motor thalamus, including the nucleus ventrooralis (VO) and the ventralis intermedius nucleus (VIM), for writer's cramp.

Methods. The authors applied thalamic DBS in five patients with writer's cramp. The inclusion criteria for the DBS trial in this disorder were a diagnosis of idiopathic writer's cramp and the absence of a positive response to medication. The exclusion criteria included significant cognitive dysfunction, active psychiatric symptoms, and evidence of other central nervous system diseases or other medical disorders. In one of the cases, DBS leads were implanted into both the globus pallidus internus and the VO/VIM, and test stimulation was performed for 1 week. The authors thus had an opportunity to compare the effects of pallidal and thalamic stimulation in this patient.

Results. Immediately after the initiation of thalamic stimulation, the neurological deficits associated with writer's cramp were improved in all five cases. Postoperatively all preoperative scale scores indicating the seriousness of the writer's cramp were significantly lower ($p < 0.001$). In the patient in whom two DBS leads were implanted, the clinical effect of thalamic stimulation was better than that of pallidal stimulation. During the thalamic stimulation, the maximum effect was obtained when stimulation was applied to both the VO and the VIM widely, compared with being applied only within the VO.

Conclusions. The authors successfully treated patients with writer's cramp by thalamic DBS. Insofar as they are aware, this is the first series in which writer's cramp has been treated with DBS. Thalamic stimulation appears to be a safe and valuable therapeutic option for writer's cramp. *(DOI: 10.3171/JNS-07/11/0977)*

Key Words • deep brain stimulation • focal dystonia • thalamotomy • writer's cramp

Writer's cramp is a representative type of idiopathic focal hand dystonia characterized by muscle cramps that accompany execution of the writing task specifically. There has been renewed interest in neurosurgical procedures for the treatment of dystonia over the past several years. In particular, DBS has received increasing attention as a therapeutic option for patients with dystonia.[4,22] This treatment modality offers several potential benefits over radiofrequency lesioning.[9] The functional location and size of the focus of stimulation can be changed and adjusted to various pathological states. Pallidal stimulation is one of the most promising new therapies for the treatment of dystonia. The VO in the thalamus, however, has been recognized as an appropriate target for radiofrequency ablation in patients with writer's cramp.[1,6,14,16,17] In this report, we describe the clinical outcome of thalamic stimulation in patients treated for writer's cramp, and we present an illustrative case that allows us to compare the effects of stimulation of the GPI and VO/VIM. In addition to these results for the clinical effectiveness, we also describe the results of an investigation regarding the best point and pattern of stimulation of the VO/VIM for writer's cramp.

Abbreviations used in this paper: AC = anterior commissure; BFMDR = Burke-Fahn-Marsden Dystonia Rating; DBS = deep brain stimulation; GPI = globus pallidus internus; MR = magnetic resonance; PC = posterior commissure; VC = ventralis caudalis nucleus; VIM = ventralis intermedius nucleus; VO = nucleus ventrooralis.

Clinical Material and Methods

Patient Population

We applied thalamic stimulation in five patients with writer's cramp. The inclusion criteria for the DBS trial were that the patient was diagnosed as having idiopathic writer's cramp and did not demonstrate evidence of a good response to medical treatment. The exclusion criteria included significant cognitive dysfunction, active psychiatric symptoms, and evidence of other central nervous system diseases or other medical disorders. The DBS lead was implanted unilaterally in all cases. In one case, two DBS leads were implanted: one each into the GPI and the VO/VIM in a single

operation. We thus had an opportunity to compare the effects of GPI and VO/VIM stimulation in this patient during a 1-week test stimulation period.

Surgical Techniques

A Leksell G head frame (Elekta Instruments) was used for the surgery. Magnetic resonance images (1-mm-thick slices) were obtained, and the AC and PC were identified on the Leksell SurgiPlan (Elekta), a customized software program for functional stereotaxy. The target was approached from a bur hole perforated anteriorly at an angle of 45 to 55° to the AC–PC line and 0 to 12.5° to the vertical plane. Three-dimensional trajectory visualization on a digitized version of the Schaltenbrand–Wahren atlas[13] was used to confirm the structures that the electrode passed.

The first trajectory was directed toward the anterior aspect of the PC, on the level of the AC–PC line, at 15 mm lateral to the midline, or 9 mm lateral to the wall of the third ventricle. Following this procedure, a semimicroelectrode recording was performed. Certain cells responding to passive joint movements of the contralateral limbs, caused by deep sensation, and cells responding to light touch on the skin of the face and contralateral limbs, caused by cutaneous sensation, appeared on this trajectory. Based on these neurophysiological findings, we defined the thalamic VIM–VC border as a vertical line on this trajectory. Cells responding to cutaneous sensation were usually observed posterior to the VIM–VC border, and semimicrostimulation produced paresthesia in such an area. The VIM–VC border determined by these observations was located 1.9 to 5.5 mm anterior to the anterior aspect of the PC. The second trajectory was directed toward the VIM–VC border, on the level of the AC–PC line, at 12 to 15 mm lateral to the midline, confirming that the trajectory was located medially to the VO/VIM–internal capsule border, as estimated by MR imaging. The locations of each thalamic nucleus were also determined using a digitalized human brain atlas adjusted to the MR image of each patient's brain.

A DBS electrode (Medtronic, Inc.) with four contact points, numbered 0 to 3 sequentially from the most distal contact (0) to the most proximal contact (3), was placed through the frontal bur hole into the thalamic VO and VIM nuclei. Each contact of the electrode was 1.5 mm long, and the contacts were 1.5 mm apart from each other. We placed Contact 0 at the VIM–VC border on the level of the AC–PC line, and 12 to 15 mm lateral to the midline, in most cases. This usually resulted in Contact 1 being located within the ventral VIM, Contact 2 within the central VIM or the posterior VO, and Contact 3 within the dorsal part of the posterior VO or the anterior VO (Fig. 1).

After implantation of the electrode, postoperative MR imaging was performed, and the stereotactic coordinates of the center of each contact were determined. The locations of the DBS electrodes and the VIM–VC border, as identified from neurophysiological data, were then reconstructed on the stereotactic coordinates of the postoperative MR imaging studies.

Stimulation Procedures

During the test stimulation period of approximately 1 week, electrical stimulation was delivered as monophasic pulses with a duration ranging from 0.05 to 0.21 msec. The frequency and intensity of stimulation were usually within the range of 90 to 185 Hz and 1.0 to 3.0 V, respectively. The DBS system, including an Implantable Pulse Generator (Medtronic), was internalized when satisfactory control of the writer's cramp was achieved during the test stimulation period. After internalization of the DBS system, we attempted to detect the most effective contact for monopolar stimulation. Subsequently, we performed bipolar stimulation with various combinations of contacts including the most effective contact of monopolar stimulation. The selection of contacts and parameters for the DBS was modified by the physicians at each follow-up visit, based on the neurological findings and the patient's own reports on improvement of the writer's cramp symptoms.

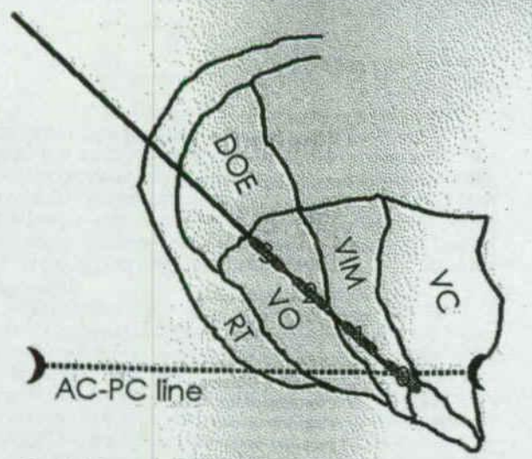

FIG. 1. Schema showing the Medtronic DBS electrode with four contact points, numbered 0 to 3 sequentially from the most distal (0) to the most proximal (3). We placed Contact 0 at the VIM–VC border on the level of the AC–PC line in most cases. This usually resulted in Contact 1 being located within the ventral VIM, Contact 2 within the central VIM or posterior VO, and Contact 3 within the dorsal part of the posterior VO or anterior VO. DOE = nucleus dorsooralis externus; RT = nucleus reticularis thalami.

Clinical Evaluation Procedures

The handwriting domain of the disability domain of the BFMDR Scale was used to evaluate patients' pre- and postoperative neurological conditions.[3] This handwriting scale is set such that normal writing receives a score of 0; slight difficulty, 1; almost illegible writing, 2; illegible writing, 3; and unable to grasp to maintain a hold on a pen, 4. Evaluations were performed using this scale preoperatively, as well as at 1 and 4 weeks and at 3, 12, and 24 months after the surgery.

We also took into consideration the patient's own subjective reports on the smoothness of writing when evaluating effects. Based on these reports, we defined the most effective combination of contacts and stimulation parameters for DBS. Also, the overall state of the letters that a patient wrote and the speed of writing were considered in the evaluation to define the appropriate mode of stimulation.

Mean results are presented ± the standard deviations.

Results

We analyzed data obtained after DBS electrode implantation in five patients with writer's cramp. The clinical characteristics and BMFDR handwriting scale scores are summarized in Table 1. The median age of the patients at surgery was 46.6 years (range 26–73 years). The median age at the onset of focal hand dystonic symptoms was 34.8 years (range 21–48 years), and the median duration of the disease was 11.8 years (range 2–25 years). In all cases the disorder was refractory to any medication. Two of the patients received botulinum toxin injection; they experienced improvement immediately after botulinum toxin injection, but the effect was short lived and did not satisfy their requirements.

As already mentioned, in the first patient we implanted two DBS leads: one each into the GPI and the VO/VIM. Based on a comparison of the results in this case, we considered thalamic stimulation to be superior to pallidal stimulation, and we adopted thalamic stimulation for use in the subsequent cases. The mean (± standard deviation) coordinates of the most distal contact of the electrodes (Contact 0) were established as 13.5 ± 1.5 mm lateral to the midline, 5.0 ± 1.1 mm anterior to the PC, and 0.9 ± 0.5 mm below the AC–PC line. We usually used one or two distal contacts as the cathode with monopolar polarity, or one distal contact as the cathode and a proximal contact as the anode with bipolar stimulation. In such situations, the stimulation parameters, including the intensity, frequency, and pulse width, were adjusted.

At 4 weeks, all five electrodes were set at 135 Hz. At 12 months, three were set at 135 Hz, one at 150 Hz, and one at 185 Hz. The mean voltage was 2.8 ± 1.3 V at 4 weeks and 2.7 ± 1.0 V at 12 months. The mean pulse width decreased from 210.0 ± 49.0 μsec at 4 weeks to 165.0 ± 57.4 μsec at 12 months. After undertaking the trial of some stimulation measures, we used bipolar stimulation in all of these patients at 12 months because of its better results. The mean preoperative handwriting score of the BFMDR instrument was 3.2 ± 0.45 in these patients. Immediately after the initiation of DBS, the score improved, to 0.4 ± 0.55, which was significantly lower than the preoperative value ($p < 0.001$, Wilcoxon t-test). The improvement in the score was maintained in subsequent evaluations at 24 months (Table 1).

We also investigated the best points for effective stimulation. We evaluated combinations of active contacts as appropriate clinical conditions for writing. The efficacy and combinations of contacts used for stimulation are summarized in Table 2. Based on our observations and each patient's subjective feelings, the bipolar stimulation of areas including VO and VIM with Cathode 0 and Anode 3 represented the most suitable combination for achieving substantial effectiveness. The mean improvement rate determined using the handwriting scale under these stimulation conditions was 91.0 ± 9.9%. The bipolar stimulation of VIM with Cathode 0 and Anode 1, however, showed an average improvement rate of 76.6 ± 22.4%, and the stimulation of VO with Cathode 2 and Anode 3 exhibited a mean improvement rate of 70.0 ± 18.3%. In the case of monopolar stimulation, the improvement rate of Stimulations 0 and 1 was 88.4 ± 16.1%; that of Stimulation 2 was 70.2 ± 18.2%; and that of Stimulation 3 was 13.2 ± 18.1%.

TABLE 1

*Clinical characteristics and BMFDR Scale scores obtained in the patients with writer's cramp**

Case No.	Age (yrs), Sex	Duration of Symptoms (yrs)	BMFDR Scale Score: Preop	4 Wks	24 Mos
1	40, M	10	3	0	0
2	42, M	2	3	0	0
3	73, M	25	4	1	1
4	26, M	5	3	0	0
5	52, M	17	3	0	0

* The BMFDR handwriting scale: 0 (best) to 4 (worst).

Stimulation with the contacts on the distal side tended to be relatively effective compared with that involving the proximal contacts in the case of monopolar stimulation. This suggests that stimulation applied to the VIM was more effective than that applied to the VO. However, the most effective mode of monopolar stimulation was relatively less effective than the most effective combination of contacts of the bipolar stimulation. Based on these results, bipolar stimulation employing the cathode on the anterior side of the VIM, with broad stimulation of the thalamic VO and VIM, appears to represent the best stimulation pattern for writer's cramp.

Illustrative Case

History. This 40-year-old man was referred to our hospital in 2001. He presented with severe stiffness in the right hand that appeared only during the handwriting task. The severity of his writing disability had gradually progressed over a period of 2 years. He had consulted a neurologist, who had diagnosed dystonic writer's cramp. This pathological condition was completely refractory to medical treatment.

Examination. Neurological examination demonstrated a severe abnormal muscle contraction in the right hand that was induced during handwriting. The stiffness and involuntary muscle contractions were present when the patient adopted the writing posture, and these deficits increased in intensity as he continued to hold a pen and write. His

TABLE 2

*Combinations of contacts used for DBS**

Contact Combination	Case No. 1	2	3	4	5
bipolar					
0(−), 3(+)	ME	ME	ME	ME	ME
1(−), 3(+)	SME	SME			
0(−), 1(+)					
1(−), 0(+)					
monopolar					
0(−), case(+)				SME	
1(−), case(+)			SME		SME
2(−), case(+)					
3(−), case(+)					

* ME = most effective; SME = second ME.